UNIVERSITY OF OKLAHOMA

GRADUATE COLLEGE

PROBING DARK ENERGY USING GALAXY CLUSTERING DATA

A DISSERTATION

SUBMITTED TO THE GRADUATE FACULTY

in partial fulfillment of the requirements for the

Degree of

DOCTOR OF PHILOSOPHY

By

CHIA-HSUN CHUANG
Norman, Oklahoma
2011

PROBING DARK ENERGY USING GALAXY CLUSTERING DATA

A DISSERTATION APPROVED FOR THE
HOMER L. DODGE DEPARTMENT OF PHYSICS AND ASTRONOMY

BY

_____

Dr. Yun Wang, Chair

_____

Dr. Eddie Baron

_____

Dr. Ronald Kantowski

_____

Dr. Chung Kao

_____

Dr. Shihshu Wei

I dedicate this thesis to my father, Wuen-Chieh Chuang, my mother, Shui-Ching Liao, my brother, Chia-Lin Chuang, my wife, Tsui-Shan Chang, and my sons, Isaac and Lucas, for their unconditional love and support.

Acknowledgements

First and foremost I would like to thank my thesis adviser, Yun Wang, for guiding me into this project. I have had a very productive and a very rich learning experience under Wang's supervising.

I would like to thank the other member in Wang's group, Maddumage Don P. Hemantha, for innumerable discussions which contributed a lot to this project.

I would like to thank Eddie Baron for teaching us using supercomputer in his course, numerical method. The data analyses involved in this project need huge computational resource. There is no way to finish this project with the few computers as we began. The computing for this project was performed at the OU Supercomputing Center for Education and Research (OSCER) at the University of Oklahoma (OU). OSCER Director Henry Neeman and staffs provided invaluable technical support.

My work has benefited from presenting in our supernova group meetings and astronomy journal club. I would like to thank all the members attending these meetings, especially Eddie Baron, Chen Bin, David Branch, Xinyu Dai, and Ronald Kantowski.

I thank my committee members Eddie Baron, David Branch, Ronald Kantowski, Chung Kao, and Shihshu Wei for their time and support.

Last but not the least, I would like to thank my host family, the Robertsons, who are John, Claudia, Olivia, and Isaac for their warm support during my stay in Norman.

iv

Contents

List of Figures

vii

List of Tables

x

Abstract

Dark energy is the most important unsolved mystery in cosmology today. Galaxy clustering provides one of the prime probes of dark energy. This work is focused on developing robust analysis techniques for interpreting galaxy clustering data. These are crucial for probing dark energy using galaxy clustering data.

First, we present a method to measure the effective distance to $z = 0.35$, $D_V(0.35)$ from the overall shape of the spherically-averaged two-point correlation function (2PCF) of the Sloan Digital Sky Survey Data Release 7 luminous red galaxy sample. We find $D_V(0.35) = 1428^{+74}_{-73}$ Mpc without assuming a dark energy model or a flat Universe. We find that the derived measurement of $r_s(z_d)/D_V(0.35) = 0.1143 \pm 0.0030$ (the ratio of the sound horizon at the drag epoch to the effective distance to $z = 0.35$) has tighter constraint and is more robust with respect to possible systematic effects. It is also nearly uncorrelated to $\Omega_m h^2$ which might be sensitive to systematic effects.

Then, we generalize the method to measure the Hubble parameter, $H(z)$, and angular diameter distance, $D_A(z)$, from the two-dimensional 2PCF, and we find $H(0.35) = 82.1^{+4.8}_{-4.9}$ km s^{-1} Mpc^{-1}, $D_A(0.35) = 1048^{+60}_{-58}$ Mpc. We also find that the derived measurements of $\{H(0.35)\, r_s(z_d),\, r_s(z_d)/D_A(0.35)\} = \{13020 \pm 530 (\text{km/s}),\, 0.1518 \pm 0.0062\}$ (with the correlation coefficient $r = -0.0584$) are nearly uncorrelated, have tighter constraints and are more robust with respect to possible systematic effects. Combining our results with the cosmic microwave background and supernova data, we obtain $\Omega_k = -0.0004 \pm 0.0070$ and $w = -0.996 \pm 0.043$ (assuming a constant dark energy equation of state).

Our results represent the first measurements of $H(z)$ and $D_A(z)$ from galaxy clustering data. Our work has significant implications for future surveys in establishing the feasibility of measuring both $H(z)$ and $D_A(z)$ from galaxy clustering data.

Chapter 1   Introduction

The discovery that the expansion of the universe is accelerating was first made by Riess et al. (1998) and Perlmutter et al. (1999), with supporting evidence for this observation strengthening over time. The cause for the observed acceleration is unknown, and is usually referred to as "the dark energy problem". Solving the mystery of the observed cosmic acceleration is one of the most exciting challenges in cosmology today.

The cosmic large-scale structure from galaxy redshift surveys provides a powerful probe of dark energy and the cosmological model that is highly complementary to the cosmic microwave background (CMB) (Bennett et al., 2003), supernovae (SNe) (Riess et al., 1998; Perlmutter et al., 1999), and weak lensing (Wittman et al., 2000; Bacon, Refregier, & Ellis, 2000; Kaiser, Wilson, & Luppino, 2000; van Waerbeke et al., 2000). The scope of galaxy redshift surveys has dramatically increased in the last decade. The PSCz surveyed $\sim 15,000$ galaxies using the Infrared Astronomical Satellite (IRAS) (Saunders et al., 2000), the 2dF Galaxy Redshift Survey (2dFGRS) obtained 221,414 galaxy redshifts (Colless et al., 2001, 2003), and the Sloan Digital Sky Survey (SDSS) has collected 930,000 galaxy spectra in the Seventh Data Release (DR7) (Abazajian et al., 2009). The ongoing galaxy surveys will probe the Universe at higher redshifts; WiggleZ is surveying 240,000 emission-line galaxies at $0.5 < z < 1$ over 1000 square degrees (Blake et al., 2009), and BOSS is surveying 1.5 million luminous red galaxies (LRGs) at $0.1 < z < 0.7$ over 10,000 square degrees (Eisenstein et al., 2011). The planned space mission Euclid will survey over 60 million emission-line galaxies at $0.5 < z < 2$ over 20,000 square degrees (Cimatti et al., 2009; Wang et al., 2010).

Large-scale structure data from galaxy surveys can be analyzed using either the power spectrum or the correlation function. Although these two methods are simple Fourier transforms of one another, the analysis processes are quite different and the results cannot be converted using Fourier transform directly because of the finite size of

the survey volume. The SDSS data have been analyzed using both the power spectrum method (see, e.g., Tegmark et al. (2004); Hutsi (2005); Padmanabhan et al. (2007); Blake et al. (2007); Percival et al. (2007, 2010); Reid et al. (2009)), and the correlation function method (see, e.g., Eisenstein et al. (2005); Okumura et al. (2008); Cabre & Gaztanaga (2008); Martinez et al. (2009); Sanchez et al. (2009); Kazin et al. (2010a); Chuang, Wang, & Hemantha (2010)). While previous work has focused on the spherically averaged two-point correlation function (2PCF), or the radial projection of the two-dimensional two point correlation function (2D 2PCF), we measure and analyze the full 2D 2PCF of SDSS LRGs in this study.

The major features in the galaxy clustering at large scales (i.e., $s > 40h^{-1}\mathrm{Mpc}$) are baryon acoustic oscillations (BAO), which were the acoustic oscillations in the photo-baryon fluid while photons and baryons were tightly coupled through Compton scattering of electrons before the last scattering of CMB photons. These oscillations froze at the decoupling of CMB photons, and imprinted their signatures in both the CMB and matter distribution. The scale of BAO corresponds to sound horizon at the drag epoch ($\sim$150 Mpc), which is precisely measured using CMB data, thus it can be used as a standard ruler. Although we are fitting the overall shape of the 2PCF instead of measuring the scale of BAO only, the primary power of the constraints comes from BAO features.

Geometric constraints on dark energy are derived from the measurement of distances. The comoving distance to an object at redshift z is given by:

$$r(z) = cH_0^{-1} |\Omega_k|^{-1/2} \mathrm{sinn}[|\Omega_k|^{1/2}\,\Gamma(z)], \qquad (1.1)$$

$$\Gamma(z) = \int_0^z \frac{dz'}{E(z')}, \qquad E(z) = H(z)/H_0$$

where $\mathrm{sinn}(x) = \sin(x)$, x, $\sinh(x)$ for $\Omega_k < 0$, $\Omega_k = 0$, and $\Omega_k > 0$ respectively; and the

expansion rate the universe $H(z)$ is given by

$$H^2(z) \equiv \left(\frac{\dot{a}}{a}\right)^2 \qquad (1.2)$$
$$= H_0^2 \left[\Omega_m(1+z)^3 + \Omega_r(1+z)^4 + \Omega_k(1+z)^2 + \Omega_X X(z)\right],$$

where Ω_m, Ω_r, Ω_k, and Ω_X are the density fractions of matter, radiation, curvature, and dark energy today, with $\Omega_m + \Omega_r + \Omega_k + \Omega_X = 1$, and the dark energy density function $X(z)$ is defined as

$$X(z) \equiv \frac{\rho_X(z)}{\rho_X(0)}, \qquad (1.3)$$

where $\rho_X(z)$ is the density of dark energy. Note that $\Omega_r \ll \Omega_m$, thus the Ω_r term is usually omitted in dark energy studies, since dark energy should only be important at late times. The angular diameter distance is given by

$$D_A(z) \equiv \frac{r(z)}{1+z}. \qquad (1.4)$$

The power of galaxy clustering as a dark energy probe lies in the fact that $H(z)$ and $D_A(z)$ can in principle be extracted simultaneously from data (Blake & Glazebrook, 2003; Seo & Eisenstein, 2003; Wang, 2006). This has not been achieved in the previous work in the analysis of real data. Okumura et al. (2008) concluded that SDSS DR3 LRG data were not sufficient for measuring $H(z)$ and $D_A(z)$; they derived constraints on cosmological parameters assuming that dark energy is a cosmological constant. Cabre & Gaztanaga (2008) measured the linear redshift space distortion parameter β, galaxy bias, and σ_8 from SDSS DR6 LRGs. Gaztanaga, Cabre, & Hui (2009) obtained a measurement of $H(z)$ by measuring the peak of the 2PCF along the line of sight. However, Kazin et al. (2010b) showed that the amplitude of the line-of-sight peak is consistent with sample variance.

First, we present the method to obtain dark energy and cosmological model constraints from the spherical-averaged 2PCF, without assuming a dark energy model or

a flat Universe. We demonstrate the feasibility of extracting $H(z)$ and $D_A(z)$ by scaling the spherical-averaged 2PCF (which leads to highly correlated measurements). And then, we obtain robust measurements of $H(z)$ and $D_A(z)$ through scaling, using the 2D correlation function measured from the same sample of SDSS DR7 LRGs (Eisenstein et al., 2001). This sample is homogeneous and has the largest effective survey volume to date for studying the quasi-linear regime (Eisenstein et al., 2005). In Chapter 2, we introduce the galaxy sample used in our study. In Chapter 3, we describe the details of our method that use the spherical-averaged 2PCF and present our results. In Chapter 4, we describe how we generalize the previous method and apply on the 2D 2PCF and the results are presented as well. We show the dark energy and curvature constraints we obtain in Chapter 5. We summarize and conclude in Chapter 6.

Chapter 2   Data

In this chapter, we introduce the observed data and the mock catalogs we use.

2.1   Galaxy Sample from SDSS

The SDSS has observed one-quarter of the entire sky and performed a redshift survey of galaxies, quasars and stars in five passbands u, g, r, i, and z with a 2.5m telescope (Fukugita et al., 1996; Gunn et al., 1998, 2006). We use the public catalog, the NYU Value-Added Galaxy Catalog (VAGC) (Blanton et al., 2005), derived from the SDSS II final public data release, Data Release 7 (DR7) (Abazajian et al., 2009). We select our LRG sample from the NYU VAGC with the flag $primTarget$ bit mask set to 32. K-corrections have been applied to the galaxies with a fiducial model (ΛCDM with $\Omega_m = 0.3$ and $h = 1$), and the selected galaxies are required to have rest-frame g-band absolute magnitudes $-23.2 < M_g < -21.2$ (Blanton & Roweis, 2007). The same selection criteria were used in previous papers (Zehavi et al., 2005; Eisenstein et al., 2005; Okumura et al., 2008; Kazin et al., 2010a). The sample we use is referred to as "DR7full" in Kazin et al. (2010a). Our sample includes 87000 LRGs in the redshift range 0.16-0.44. The average weighted redshift is 0.33.

Spectra cannot be obtained for objects closer than 55 arcsec within a single spectroscopic tile due to the finite size of the fibers. To correct for these "collisions", the redshift of an object that failed to be measured would be assigned to be the same as the nearest successfully observed one. Both fiber collision corrections and K-corrections have been made in NYU-VAGC (Blanton et al., 2005). The collision corrections applied here are different from what has been suggested in Zehavi et al. (2005). However, the effect should be small since we are using relatively large scale which are less affected by the collision corrections.

We construct the radial selection function as a cubic spline fit to the observed number density histogram with the width $\Delta z = 0.01$ (see Fig. 2.1). The NYU-VAGC provides

5
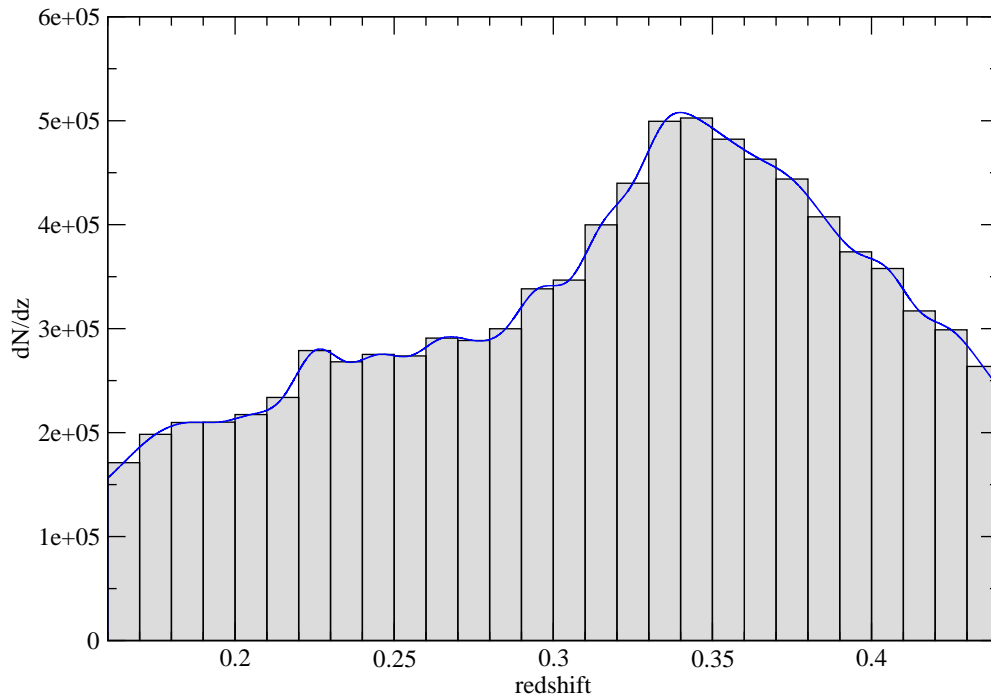
Figure 2.1: The radial selection function of the LRG sample used in this study. The gray bars are computed from the sample and the blue line is the cubic spline fit of these bar values. We compute the radial selection function in the form of the number of galaxies per unit redshift instead of the number density in comoving coordinate, so that we don't need to assume a fiducial model while generating the random catalog with the radial selection function.

the description of the geometry and completeness of the survey in terms of spherical polygons. Although the completeness of VAGC is determined based on the main galaxies (Strauss et al., 2002), we adopt it as the angular selection function of our sample since the main galaxies and LRGs should have similar angular selection functions (see the appendix of Zehavi et al. 2005). We drop the regions with completeness below 60% to avoid unobserved plates (Zehavi et al., 2005). The Southern Galactic Cap region is also dropped.

2.2 Mock Catalogs from LasDamas Simulation

Large Suite of Dark Matter Simulations (LasDamas) is a project to run a large suite of cosmological N-body simulations that follow the evolution of dark matter in the universe. The focus is to obtain adequate resolution in many large boxes, rather than a single realization at high resolution. This will result in an enormous volume appropriate for statistical studies of galaxies and halos.

The LasDamas simulations are designed to model the clustering of Sloan Digital Sky Survey (SDSS) galaxies in a wide luminosity range, with the goal of assisting in the modeling of galaxy clustering measurements. Specifically, the simulations are used to construct detailed mock galaxy catalogs by placing artificial galaxies inside dark matter halos using a Halo Occupation Distribution (Berlind and Weinberg , 2002) with parameters fit from the respective SDSS galaxy samples.

Chapter 3 Measurements from Spherically Averaged Two-Point Correlation Function

In this chapter, we describe the measurement of the spherically-averaged two-point correlation function (1D 2PCF) from the observational data, construction of the theoretical prediction, and the likelihood analysis that leads to constraints on dark energy and cosmological parameters.

3.1 Methodology

3.1.1 Measuring the Two-point Correlation Function

We calculate the comoving distances to every galaxy by assuming a fiducial model, ΛCDM with $\Omega_m = 0.25$. We use the two-point correlation function estimator given by Landy and Szalay (Landy & Szalay, 1993):

$$\xi(s) = \frac{DD(s) - 2DR(s) + RR(s)}{RR(s)}, \tag{3.1}$$

where DD, DR, and RR represent the normalized data-data, data-random, and random-random pair counts respectively in a distance range. The bin size we use in this study is $5h^{-1}$Mpc. This estimator has minimal variance for a Poisson process. Random data should be generated according to the radial and angular selection functions of the data. One can reduce the shot noise due to random data by increasing the number of random data. The number of random data we use is 10 times that of the real data. While calculating the pair counts, we assign each data point a radial weight of $1/[1 + n(z) \cdot P_w]$, where $n(z)$ is the radial selection function and $P_w = 4 \cdot 10^4 \ h^{-3}$Mpc^3 as in Eisenstein et al. (2005). The observed correlation function is shown in Fig. 3.1.
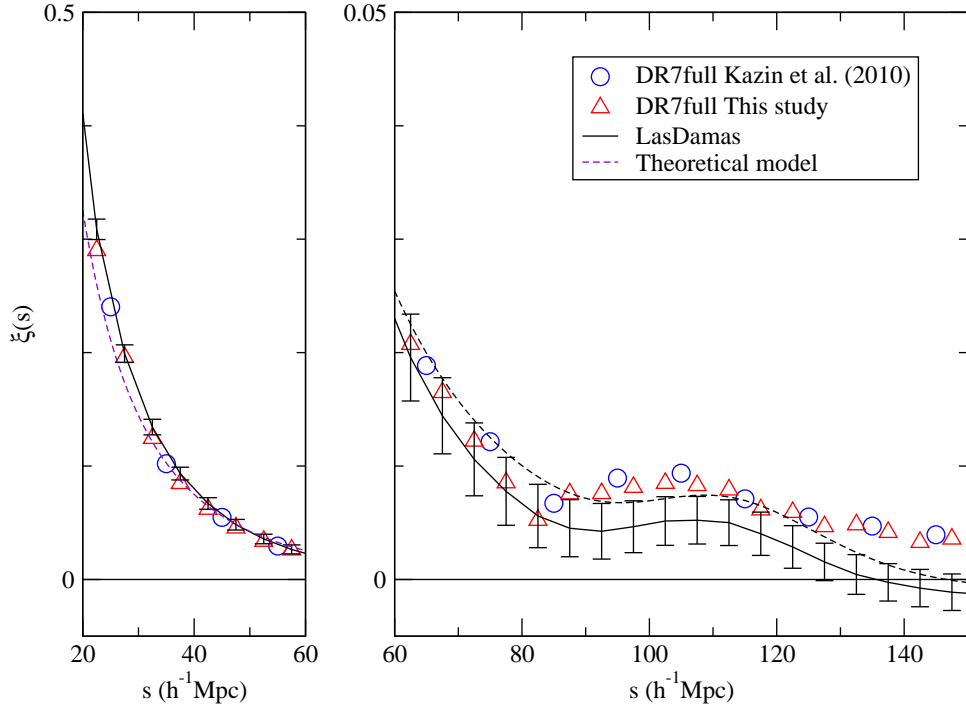
Figure 3.1: The spherically-averaged two-point correlation function measured from the SDSS DR7 data. The red triangles are the correlation function computed with the LRG sample described in Chap. 2. The green circles are taken from Kazin et al. 2010a in which the same fiducial model is used (ΛCDM with $\Omega_m = 0.25$) but the bin size they use is $10h^{-1}$Mpc. Our result shows excellent agreement with that of Kazin et al. 2010a. The black line is the average correlation function from LasDamas mock catalogs. The error bars are the square roots of the diagonal elements of the covariance matrix we have derived (see Sec. 3.1.3). The violet dashed line is the mean model from our MCMC likelihood analysis ($\Omega_m h^2 = 0.105, \Omega_b h^2 = 0.0225, n_s = 0.978, D_V(0.35) = 1432$Mpc). Note that an MCMC analysis does not result in an accurate best fit model (Lewis & Bridle, 2002).

3.1.2 Theoretical Two-Point Correlation Function

We compute the linear power spectra at $z = 0.33$ by using CAMB (Lewis, Challinor, & Lasenby, 2000). To include the effect of non-linear structure formation and peculiar velocities on the BAOs, we calculate the dewiggled power spectrum

$$P_{dw}(k) = P_{lin}(k) \exp\left(-\frac{k^2}{2k_\star^2}\right) + P_{nw}(k)\left[1 - \exp\left(-\frac{k^2}{2k_\star^2}\right)\right], \tag{3.2}$$

where $P_{lin}(k)$ is the linear power spectrum, $P_{nw}(k)$ is the no-wiggle or pure CDM power spectrum calculated with the formula in Eisenstein & Hu (1998),

$$P_{nw}(k) = Ak^{n_s}T_0(q), \tag{3.3}$$

where A can be determined by matching $P_{nw}(k)$ with $P_{lin}(k)$ at $k \sim 0$ and

$$
\begin{aligned}
T_0(q) &= \frac{L_0}{L_0 + C_0 q^2}, \\
L_0(q) &= \ln(2e + 1.8q), \\
C_0(q) &= 14.2 + \frac{731}{1 + 62.5q},
\end{aligned}
\tag{3.4}
$$

where

$$q = \frac{k}{h\,\mathrm{Mpc}^{-1}}\frac{\Theta_{2.7}^2}{\Omega_m h}, \tag{3.5}$$

where $\Theta_{2.7}$ is the temperature of CMB divided by 2.7, and $k_\star$ (in Eq. 3.2) is marginalized over with a flat prior over the range of 0.09 to 0.13[1] We next use the Smith et al. (2003) package, *halofit*, to compute the non-linear power spectrum:

$$r_{halofit}(k) \equiv \frac{P_{halofit,nw}(k)}{P_{nw}(k)} \tag{3.6}$$

$$P_{nl}(k) = P_{dw}(k)r_{halofit}(k), \tag{3.7}$$

---

[1]Although $k_\star$ can be computed by renormalization perturbation theory (Crocce & Scoccimarro, 2006; Matsubara, 2007), doing so requires knowing the amplitude of the power spectrum, which is also marginalized over in this study.

where $P_{halofit,nw}(k)$ is the power spectrum from applying *halofit* on the no-wiggle power spectrum and $P_{nl}(k)$ is the non-linear power spectrum. We compute the theoretical two-point correlation function by Fourier transforming the non-linear power spectrum. We show an example of the effect of applying dewiggle and *halofit* to the correlation function in Fig. 3.2. Clearly, the damping of BAO is accurately described by the dewiggled linear correlation function. Additional nonlinear effects are only important on very small scales.

The parameter set we use to compute the theoretical correlation function is $\{D_V(z), \Omega_m h^2, \Omega_b h^2, n_s, k_\star\}$, where Ω_m and Ω_b are the density fractions of matter and baryons, n_s is the power law index of the primordial matter power spectrum, h is the dimensionless Hubble constant ($H_0 = 100h$ km s^{-1}Mpc^{-1}), and $D_V(z)$ is defined by

$$D_V(z) \equiv \left[(1+z)^2 D_A^2 \frac{cz}{H(z)} \right]^{\frac{1}{3}}, \tag{3.8}$$

where $H(z)$ and $D_A(z)$ are the Hubble parameter and the angular diameter distance at the redshift, z. We set $h = 0.7$ while calculating the non-linear power spectra. The dark energy and curvature dependence are absorbed by the effective distance, $D_V(z)$. Thus we are able to extract constraints from data without assuming a dark energy model and cosmic curvature.

3.1.3 Covariance Matrix

We use the mock catalogs from the LasDamas simulations[2] (McBride et al., in preparation) to estimate the covariance matrix of the observed correlation function. LasDamas provides mock catalogs matching SDSS main galaxy and LRG samples. We use the LRG mock catalogs from the LasDamas gamma release with the same cuts as the SDSS LRG volume-limited sample, $-23.2 < M_g < -21.2$ and $0.16 < z < 0.44$. We have diluted the mock catalogs to match the radial selection function of the observed data by randomly selecting the mock galaxies according to the number density of the data sample. We cal-

---

[2]http://lss.phy.vanderbilt.edu/lasdamas/
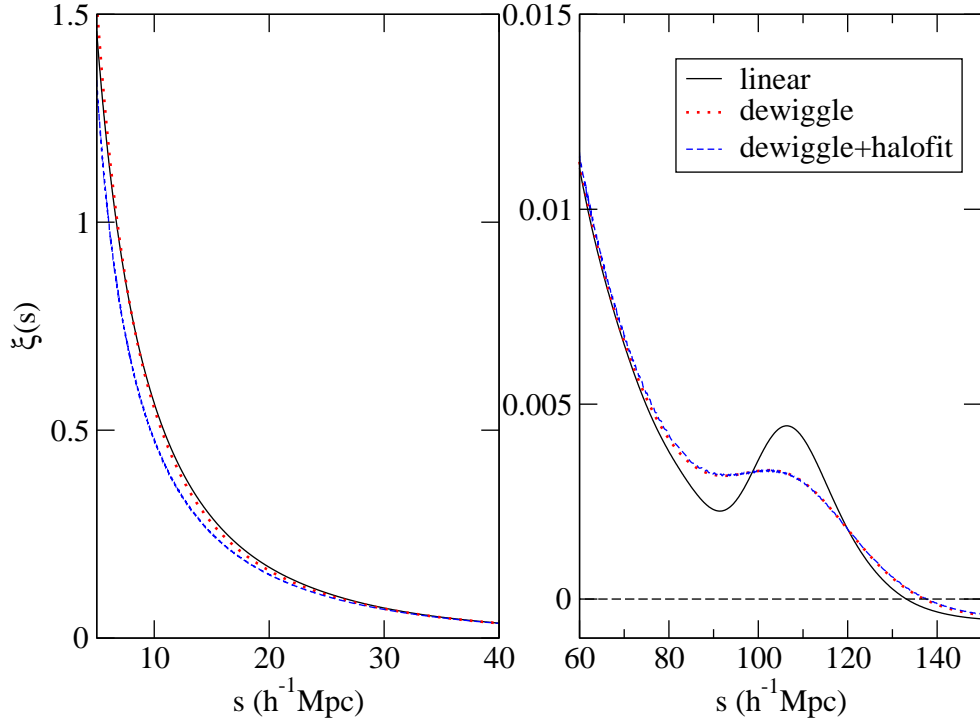
Figure 3.2: An example of the effect of applying dewiggle and *halofit* to the correlation function. The black solid line is the linear correlation function without applying dewiggle and *halofit* yet. The red dotted line is the dewiggled linear correlation function. The green dashed line is the dewiggled correlation function including nonlinear effects calculated using *halofit*. The damping of BAO is accurately described by the dewiggled linear correlation function. Additional nonlinear effects are only important on very small scales.

culate the spherical-averaged correlation functions of the mock catalogs and construct the covariance matrix as

$$C_{ij} = \frac{1}{N-1} \sum_{k=1}^{N} (\bar{\xi}_i - \xi_i^k)(\bar{\xi}_j - \xi_j^k), \tag{3.9}$$

where N is the number of the mock catalogs, $\bar{\xi}_m$ is the mean of the mth bin of the mock correlation functions, and ξ_m^k is the value of mth bin of the kth mock correlation function.

The mock catalogs derived from N-body simulations require long computing times and are very limited in availability. It is interesting to investigate whether there is an easier, faster, and cheaper way to construct mock catalogs which could work as well as those derived from N-body simulation. Towards this end, we have created 500 lognormal(LN) mock catalogs (Coles & Jones, 1991; Percival, Verde, & Peacock, 2004), and computed the spherically-averaged correlation functions from these. The details involved in creating LN mock catalogs are described in Appendix A. We compare the correlation functions from the LasDamas mock catalogs and LN mock catalogs in Fig. 3.3; the error bars indicate the square roots of the diagonal elements of the covariance matrixes. We also show the normalized covariance matrixes in Fig. 3.4 and 3.5. Clearly, the results from the LasDamas mocks and our LN mocks are very similar to each other. In particular, the input correlation function is accurately recovered by analyzing the LN mock catalogs. Note that the LN mocks give larger errors on all scales, and on scales smaller than $\sim 60h^{-1}$Mpc, the LN mock catalogs give much larger errors than the LasDamas mock catalogs (see Fig. 3.6).

We use the covariance matrix computed from the LasDamas SDSS mock catalogs, since these are more realistic than the lognormal mock catalogs, and give smaller errors for the measured correlation function. It is interesting to note that in the absence of mock catalogs derived from cosmological N-body simulations, lognormal catalogs can be used for a conservative estimate of the covariance matrix of the correlation function.

13
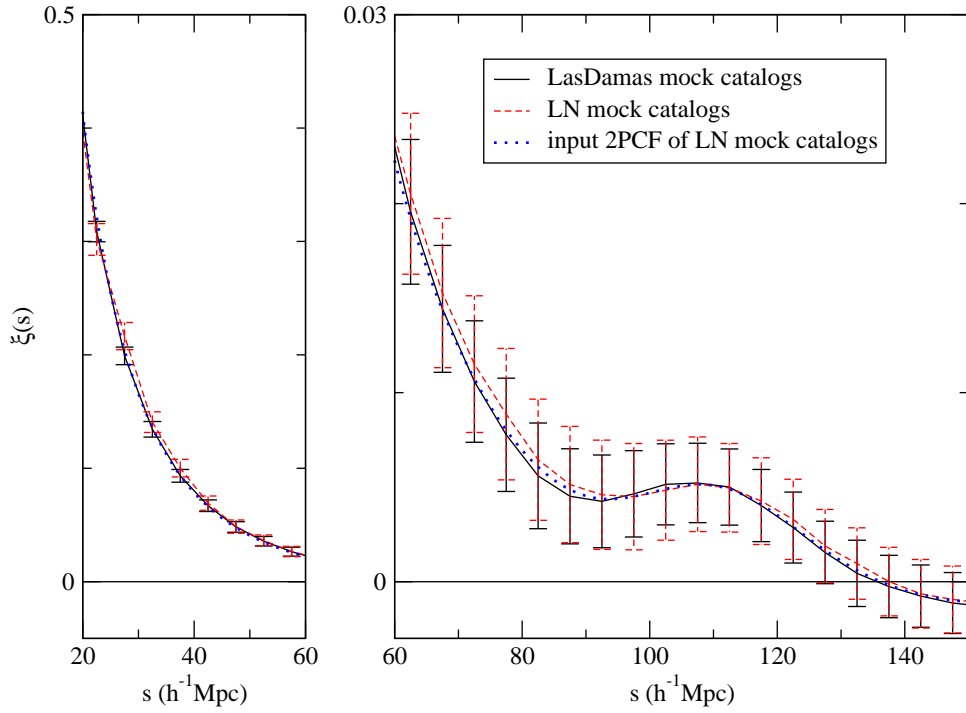
Figure 3.3: Spherical-averaged 2PCF of the mock catalogs. The black solid line is computed from the LasDamas mock catalogs. The red dashed line is computed from our lognormal mock catalogs. The error bars are the square roots of the diagonal elements of the covariance matrixes. The green dotted line is the input 2PCF for our lognormal mock catalogs.

14
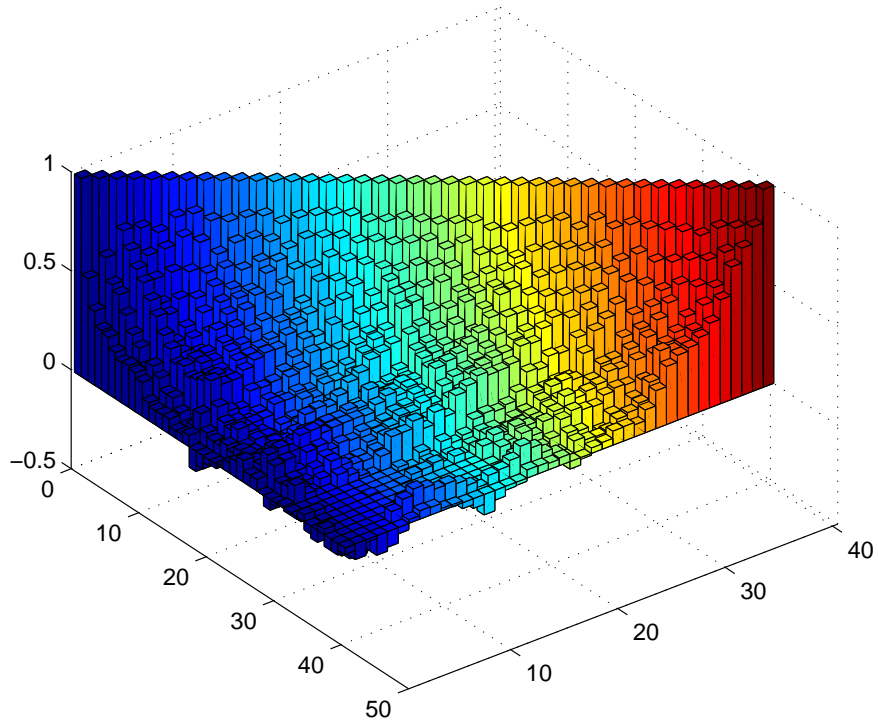
Figure 3.4: The normalized covariance matrix computed from 160 LasDamas mock catalogs. We show the covariance among 40 bins from $0 < s < 200h^{-1}\mathrm{Mpc}$ with bin size $5h^{-1}\mathrm{Mpc}$.
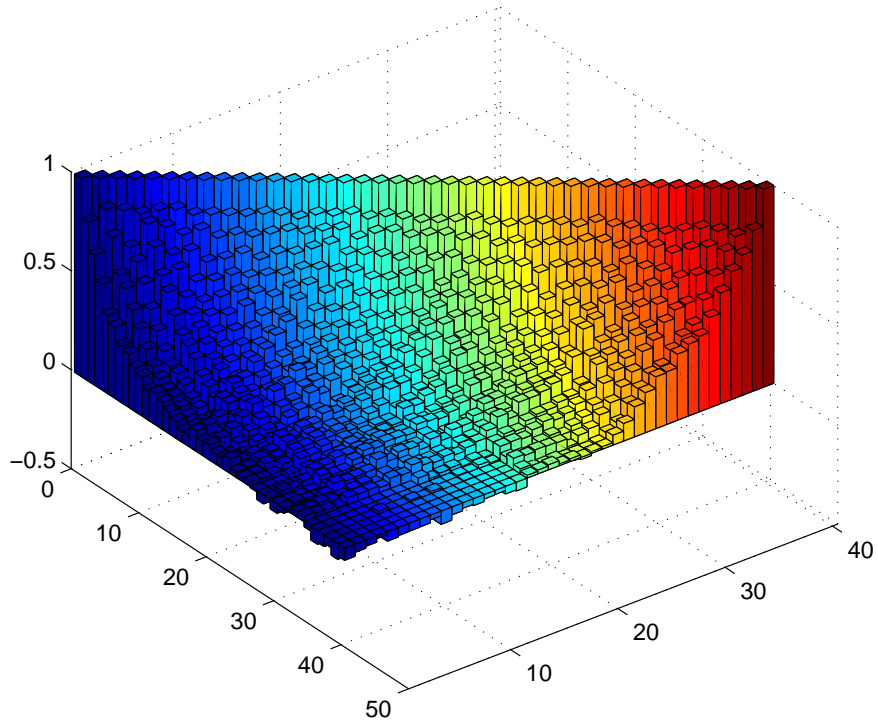
Figure 3.5: The normalized covariance matrix computed from 500 lognormal mock catalogs. We show the covariance among 40 bins between the scale range, $0 < s < 200h^{-1}\text{Mpc}$, with the bin size, $5h^{-1}\text{Mpc}$.
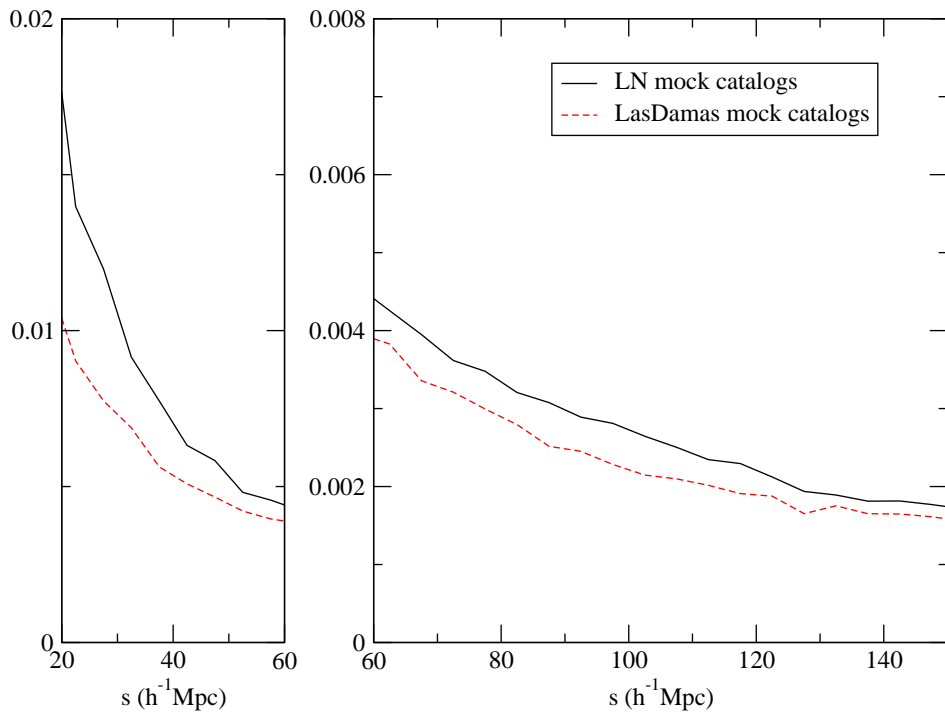
Figure 3.6: Square roots of the diagonal elements of the covariance matrixes. The black dashed line is computed from the LasDamas mock catalogs. The red solid line is computed from lognormal mock catalogs we create. One can see that LN mock catalogs have larger covariance at smaller scale and two lines are close at larger scale.

3.1.4 Likelihood

The likelihood is taken to be proportional to $\exp(-\chi^2/2)$, and χ^2 is given by

$$\chi^2 \equiv \sum_{i,j=1}^{N_{bins}} [\xi_{th}(s_i) - \xi_{obs}(s_i)] \, C_{ij}^{-1} \, [\xi_{th}(s_j) - \xi_{obs}(s_j)] \tag{3.10}$$

where N_{bins} is the number of bins used, ξ_{th} is the theoretical correlation function of a model, and ξ_{obs} is the observed correlation function. Note that $\xi_{th}(s_i)$ depends on $\{D_V(z), \Omega_m h^2, \Omega_b h^2, n_s\}$.

In principle, we should recalculate the observed correlation function while computing the χ^2 for different models. However, since we don't consider the entire scale range of the correlation function (we only consider $s = 40 - 120\ h^{-1}$Mpc in this study), we might include or exclude different data pairs for different models which would render χ^2 values arbitrary. Therefore, instead of recalculating the observed correlation function, we apply the inverse operation to the theoretical correlation function to move the parameter dependence from the data to the model, thus preserving the number of galaxy pairs used in the likelihood analysis.

Let us define T as the operator converting the measured correlation function from the fiducial model to another model, i.e.,

$$\xi_{obs}(s) = T(\xi_{obs}^{fid}(s)). \tag{3.11}$$

where $\xi_{obs}^{fid}(s)$ is the observed correlation function assuming the fiducial model. This allows us to rewrite χ^2 as

$$\chi^2 \equiv \sum_{i,j=1}^{N_{bins}} \left\{ T^{-1} [\xi_{th}(s_i)] - \xi_{obs}^{fid}(s_i) \right\} C_{fid,ij}^{-1} \cdot$$
$$\cdot \left\{ T^{-1} [\xi_{th}(s_j)] - \xi_{obs}^{fid}(s_j) \right\}, \tag{3.12}$$

where we have used Eqs.(3.9) and (3.11).

To find the operator T, note that the fiducial model is only used in converting redshifts into distances for the galaxies in our data sample. In the analysis of galaxy clustering, we only need the separation of a galaxy pair, and not the absolute distances to the galaxies. For a thin redshift shell, we can convert the separation of one pair of galaxies from the fiducial model to another model by performing the scaling (see, e.g., Seo & Eisenstein (2003))

$$s' = \sqrt{\left(s\cos\theta\frac{H^{fid}(z)}{H(z)}\right)^2 + \left(s\sin\theta\frac{D_A(z)}{D_A^{fid}(z)}\right)^2}, \qquad (3.13)$$

where θ is the angle between the radial direction and the direction of the line connecting the pair of galaxies.

Eisenstein et al. (2005) argued that we can use one rescaling parameter, $D_V(z)$, to convert the observed correlation function from the fiducial model to another model as long as the new model is not very different from the fiducial one, and the redshift range of the sample is not large. Then the separation of one pair of galaxies is converted from the fiducial model to another by

$$s' = \frac{D_V(z)}{D_V^{fid}(z)}s. \qquad (3.14)$$

In this section, we discuss methods with one and two rescaling parameters, and show that these two methods are equivalent for spherically-averaged data when certain conditions hold (see Sec. 3.1.4).

Using One Rescaling Parameter

From eq. (3.14), the observed correlation function with the different model can be written as follows:

$$\xi_{obs}(s) = \xi_{obs}^{fid}\left(\frac{D_V^{fid}(z_{eff})}{D_V(z_{eff})}s\right), \qquad (3.15)$$

where z_{eff} is the effective redshift of the sample and $D_V(z)$ is defined by Eq.(3.8).

The effective redshift we use in this study is $z_{eff} = 0.31$. Since the results are

insensitive to z_{eff} (see Sec. 3.3), we rescale our result to $z_{eff} = 0.35$ for comparing with previous work. Eq. (3.15) can be rewritten as

$$\xi_{obs}^{fid}(s) = T^{-1}(\xi_{obs}(s)) = \xi_{obs}\left(\frac{D_V(z_{eff})}{D_V^{fid}(z_{eff})}s\right). \tag{3.16}$$

We can apply the same inverse rescaling operation to the theoretical correlation function:

$$T^{-1}(\xi_{th}(s)) = \xi_{th}\left(\frac{D_V(z_{eff})}{D_V^{fid}(z_{eff})}s\right). \tag{3.17}$$

χ^2 can be calculated by substituting eq. (3.17) into eq. (3.12).

Using Two Rescaling Parameters

From eq. (3.13), we can convert the spherically-averaged correlation function from some model to the fiducial model by

$$\xi_{obs}^{fid}(s) = T^{-1}(\xi_{obs}(s))$$
$$= \int_0^\pi d\theta w(s,\theta)\times$$

$$\xi_{obs}\left(\sqrt{\left(s\cos\theta\frac{H^{fid}(z)}{H(z)}\right)^2 + \left(s\sin\theta\frac{D_A(z)}{D_A^{fid}(z)}\right)^2}\right), \tag{3.18}$$

where the weighting function $w(r,\theta)$ is given by

$$w(s,\theta) = \frac{n_{DD}(s,\theta)}{\int_0^\pi d\theta n_{DD}(s,\theta)}, \tag{3.19}$$

where $n_{DD}(s,\theta)$ is the number density of the data pairs. We define inverse operation, T^{-1}, directly since T is not necessary in our calculation. We now apply the inverse

operation to the theoretical correlation function:

$$T^{-1}(\xi_{th}(s)) = \int_0^\pi d\theta w(s,\theta) \times$$

$$\xi_{th}\left(\sqrt{\left[s\cos\theta\frac{H^{fid}(z)}{H(z)}\right]^2 + \left[s\sin\theta\frac{D_A(z)}{D_A^{fid}(z)}\right]^2}\right). \tag{3.20}$$

χ^2 can be calculated by substituting eq. (3.20) into eq. (3.12).

Equivalence of Using One and Two Rescaling Parameters for Spherically-Averaged Data

We now show that using one and two rescaling parameters while calculating the spherically-averaged correlation function are equivalent to first order in approximation. If the size of the survey is much larger than the scales of interest, $n_{DD}(s,\theta)$ would be proportional to $s\sin\theta$. Hence

$$w(s,\theta) \sim \frac{s\sin\theta}{\int_0^\pi s\sin\theta d\theta} = \frac{\sin\theta}{2}. \tag{3.21}$$

Next, if the model is close to the fiducial model, we can just consider the first order terms of D_V/D_V^{fid}, H^{fid}/H, and D_A/D_A^{fid} which can be written as following:

$$\frac{D_V}{D_V^{fid}} \simeq 1 + \delta_V, \quad \frac{H^{fid}}{H} \simeq 1 + \delta_r, \quad \frac{D_A}{D_A^{fid}} \simeq 1 + \delta_a, \tag{3.22}$$

where $|\delta_V|, |\delta_r|, |\delta_a| \ll 1$. From the definition of D_V (see Eq.[3.8]), one can obtain a simple relation, $3\delta_V \simeq \delta_r + 2\delta_a$. Let's consider a power law correlation function:

$$\xi_{th}(s) = s^p, \tag{3.23}$$

21

where p is a real number. Eq.(3.20) can be rewritten as

$$
\begin{aligned}
T^{-1}&(\xi_{th}(s)) \\
&\simeq \int_0^\pi d\theta \frac{\sin\theta}{2} \left(\sqrt{[s\cos\theta(1+\delta_r)]^2 + [s\sin\theta(1+\delta_a)]^2} \right)^p \\
&\simeq \frac{s^p}{2} \int_0^\pi d\theta \sin\theta \left[\cos^2\theta(1+2\delta_r) + \sin^2\theta(1+2\delta_a) \right]^{\frac{p}{2}} \\
&\simeq \frac{s^p}{2} \int_0^\pi d\theta \sin\theta \left[1 + p(\cos^2\theta\delta_r + \sin^2\theta\delta_a) \right] \\
&= s^p \left[1 + p\frac{\delta_r + 2\delta_a}{3} \right] \\
&\simeq s^p(1 + p\delta_V) \\
&\simeq \left(\frac{D_V}{D_V^{fid}} s \right)^p \\
&= \xi_{th}\left(\frac{D_V}{D_V^{fid}} s \right)
\end{aligned}
\tag{3.24}
$$

The proof can be generalized to any function which can be expressed as

$$
\xi_{th}(s) = s^{p_1} + s^{p_2} + s^{p_3} + ...
\tag{3.25}
$$

where p_i are real numbers.

To measure the spherically-averaged correlation function, we have shown that using one rescaling parameter, D_V, and two rescaling parameters, H and D_A, are equivalent as long as the scales of interest are relatively small compared to the survey length scale, and the constraint on D_V is tight enough. A similar statement can be made for the spherically-averaged power spectrum analysis.

3.1.5 Markov Chain Monte-Carlo Likelihood Analysis

We use CosmoMC (Lewis & Bridle, 2002) in a Markov Chain Monte-Carlo likelihood analysis. The main parameter space that we explore is $\{\Omega_m h^2,\ \Omega_b h^2,\ n_s,\ D_V(z_{eff}),$ $k_\star\}$ and the prior ranges are $\{(0.025, 0.3),\ (0.01859, 0.02657),\ (0.865, 1.059),\ (725, 1345),$

$(0.09, 0.13)\}$ respectively. The dependence on h, the curvature, and dark energy parameters are absorbed into $D_V(z_{eff})$.

We marginalize over the amplitude of the correlation function; this is equivalent to marginalizing over galaxy bias$\times\sigma_8 \times r_\beta$, where σ_8 is the matter power spectrum normalization parameter and r_β is the linear ratio between the correlation function in the redshift space and real space which can be derived from the linear redshift distortion parameter (Kaiser, 1987). Since the LRG data alone cannot give tight constraints on $\Omega_b h^2$ and n_s, we apply flat priors ($7\sigma_{WMAP}$) on them which are wide enough so that CMB constraints will not be double counted. In other words, the effect from the wide flat priors could be ignored when combining our final results with CMB data.

3.2 Results

In this section, we present the model independent measurements of the parameters we explore, $\{D_V(0.35),\ \Omega_m h^2\}$, obtained by using the method described in previous sections. Although, the effective redshift we use is 0.33, the average weighted redshift, we rescale all our results to $z_{eff} = 0.35$ for comparing with previous work easily by

$$D_V(0.35) = D_V(0.33)\frac{D_{V,fid}(0.35)}{D_{V,fid}(0.33)} = 1.054 D_V(0.33). \tag{3.26}$$

We have checked that the results is insensitive to the effective redshift in Sec. 3.3. We derive the model independent measurements of H and D_A for comparison with 2D results.

We validate our method by applying it to the LasDamas mock catalogs, and find that our measurements are consistent with the input parameters of the simulations.

3.2.1 Model Independent Constraints on $D_V(0.35)$

Without assuming a dark energy model or a flat Universe, we find that $D_V(0.35)$ $= 1428^{+74}_{-73}$ Mpc and $r_s(z_d)/D_V(0.35) = 0.1143 \pm 0.0030$, where $r_s(z_d)$ is the comoving

	mean	σ	lower	upper
$D_V(0.35)$(Mpc)	1428	74	1355	1502
$\Omega_m h^2$	0.105	0.016	0.090	0.121
$r_s(z_d)/D_V(0.35)$	0.1143	0.0033	0.1113	0.1173
$A(0.35)$	0.439	0.020	0.419	0.459

Table 3.1: Measured cosmological parameters with flat prior $0.01859 < \Omega_b h^2 < 0.02657$ and $0.865 < n_s < 1.059$ ($\pm 7\sigma_{WMAP7}$). The standard deviations and the marginalized bounds (68%) are listed as well.

sound horizon at the drag epoch calculated with the eq. (6) in Eisenstein & Hu (1998).

Fig. 3.7 shows one and two-dimensional marginalized contours of the parameters, $\{D_V(0.35), \Omega_m h^2, r_s(z_d)/D_V(0.35), A(0.35)\}$, where

$$A(z) \equiv D_V(z) \frac{\sqrt{\Omega_m H_0^2}}{cz}. \tag{3.27}$$

The measurements and the covariance matrix are listed in Table 3.1 and 3.2. The best fit model from the MCMC likelihood analysis has $\chi^2 = 6.32$ for 16 bins of data used (in the scale range of $40\,h^{-1}$Mpc$< s < 120\,h^{-1}$Mpc with the bin size $= 5\,h^{-1}$Mpc), for a set of 6 parameters (including the overall amplitude of the correlation function).

The scale range of the correlation function we have selected is $s = 40 - 120\,h^{-1}$Mpc. In this range, the scale dependence of the redshift distortion and galaxy bias is small. We cut the tail of the correlation function at $s = 120\,h^{-1}$Mpc because the high tail (large correlation at large scales) cannot be fitted to any conventional model, and could be due to systematic error or sample variance (see further discussion in Sec. 3.3).

At this point, we assume the high tail is simply due to sample variance, and might disappear when much larger data sets become available. Unlike previous analyses by other groups, we apply very weak flat priors ($\pm 7\sigma_{WMAP7}$) on $\Omega_b h^2$ and n_s instead of fixing them to the best fit values from CMB data.
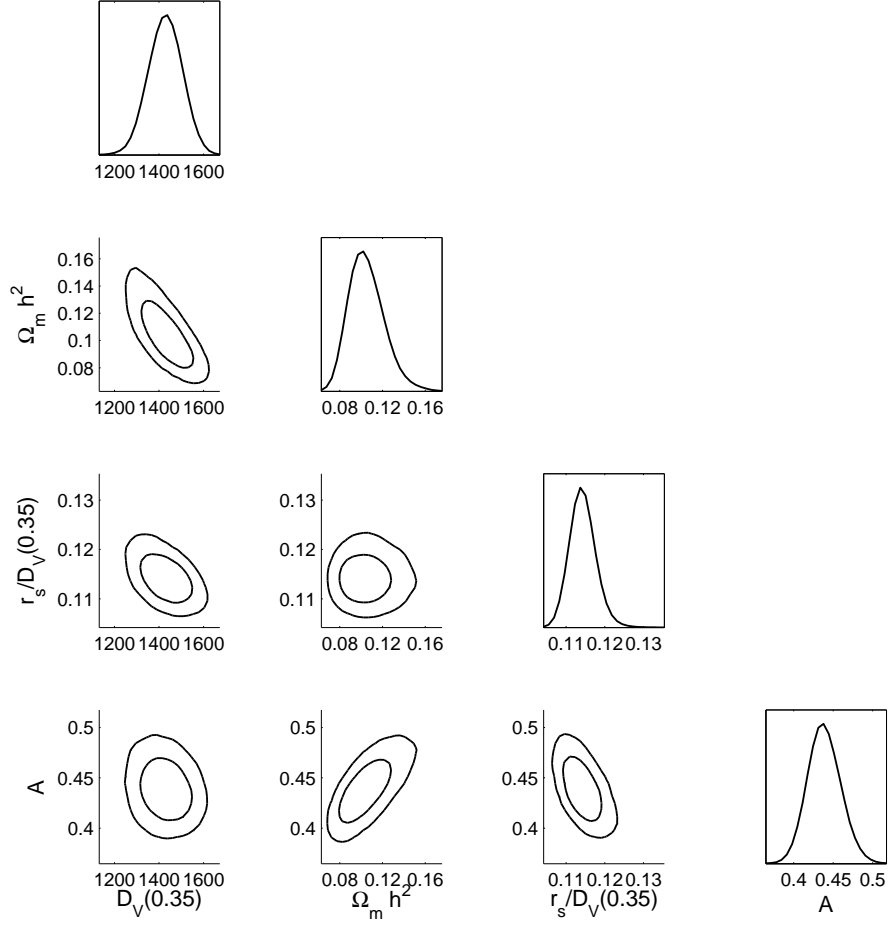
Figure 3.7: 2D marginalized contours (68% and 95% C.L.) for $D_V(0.35)$, $\Omega_m h^2$, $r_s(z_d)$ / $D_V(0.35)$, and $A(0.35)$. The diagonal panels represent the marginalized probabilities.

	$D_V(0.35)$	$\Omega_m h^2$	$r_s(z_d)/D_V(0.35)$	$A(0.35)$
$D_V(0.35)$	1	-0.7890	-0.5561	-0.1727
$\Omega_m h^2$	-0.7890	1	0.0056	0.7305
$r_s(z_d)/D_V(0.35)$	-0.5561	00056	1	-0.6181
$A(0.35)$	-0.1727	0.7305	-0.6181	1

Table 3.2: Normalized covariance matrix with flat prior $0.01859 < \Omega_b h^2 < 0.02657$ and $0.865 < n_s < 1.059$ ($\pm 7\sigma_{WMAP7}$).

	mean	σ	lower	upper
$H(0.35)$ (km s^{-1}Mpc^{-1})	83	17	68	96
$D_A(0.35)$ (Mpc)	1089	93	1002	1182
$\Omega_m h^2$	0.105	0.017	0.089	0.122
$H(0.35)\, r_s(z_d)$	13500	2700	11200	15500
$r_s(z_d)/D_A(0.35)$	0.151	0.012	0.140	0.161
$A(0.35)$	0.432	0.026	0.408	0.457

Table 3.3: Measured cosmological parameters with flat prior $0.01859 < \Omega_b h^2 < 0.02657$ and $0.865 < n_s < 1.059$ ($\pm 7\sigma_{WMAP7}$). The standard deviations and the marginalized bounds (68%) are listed as well.

3.2.2 Model independent measurements of $H(0.35)$ and $D_A(0.35)$

In this section, we apply the method with two scaling parameters described in sec 3.1.4 to measure H and D_A. We obtain the model independent measurements, $H(0.35) = 83^{+13}_{-15}$ km s^{-1}Mpc^{-1} and $D_A(0.35) = 1089^{+93}_{-87}$ Mpc, from the LRG data alone (see Table 3.3). Table 3.4 shows the normalized covariance matrix of $\{H(0.35),\, D_A(0.35),\, \Omega_m h^2,\, H(0.35)\, r_s(z_d),\, r_s(z_d)/D_A(0.35), A(0.35)\}$, and Fig. 3.8 shows the 2D marginalized contours of this parameter set.

Although using two rescaling parameters on the spherically-averaged correlation function cannot give better constraints on the cosmological parameters, it gives the model independent measurements of H and D_A which cannot be derived directly from the measurement of D_V. These can be compared to our result for the two-dimensional two-point correlation function in Chapter 4, $H(0.35) = 82.1^{+4.8}_{-4.9}$ km s^{-1} Mpc^{-1} and $D_A(0.35) = 1048^{+60}_{-58}$ Mpc. Not surprisingly, information is lost in the spherical averaging of data.

3.2.3 Validation Using Mock Catalogs

In order to validate our method, we have applied it to the mean of the spherically-averaged 2PCF of the LasDamas mock catalogs. Again, we apply the flat and wide priors ($\pm 7\sigma_{WMAP7}$) on $\Omega_b h^2$ and n_s, centered on the input values of the simulation ($\Omega_b h^2 = 0.0196$ and $n_s = 1$).

	$H(0.35)$	$D_A(0.35)$	$\Omega_m h^2$	$H(0.35)r_s(z_d)$	$\frac{r_s(z_d)}{D_A(0.35)}$	$A(0.35)$
$H(0.35)$	1	0.4028	0.2133	0.9744	-0.5733	-0.3460
$D_A(0.35)$	0.4028	1	-0.4829	0.5300	-0.8440	-0.1210
$\Omega_m h^2$	0.2133	-0.4829	1	0.0025	-0.0139	0.6035
$H(0.35)r_s(z_d)$	0.9744	0.5300	0.0025	1	-0.5861	-0.4723
$\frac{r_s(z_d)}{D_A(0.35)}$	-0.5733	-0.8440	-0.0139	-0.5861	1	-0.2033
$A(0.35)$	-0.3460	0.0908	0.6035	-0.4723	-0.2033	1

Table 3.4: Normalized covariance matrix with flat prior $0.01859 < \Omega_b h^2 < 0.02657$ and $0.865 < n_s < 1.059$ ($\pm 7\sigma_{WMAP7}$).
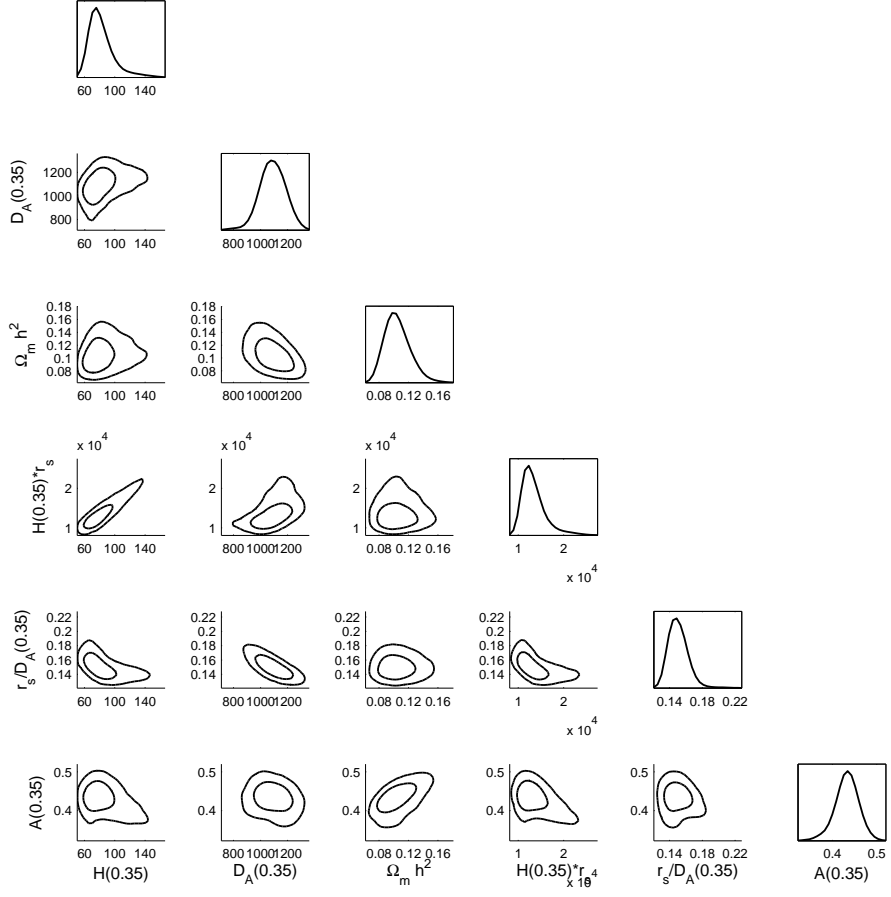
Figure 3.8: 2D marginalized contours for 68% and 95% for $H(z = 0.35)$, $D_A(z = 0.35)$, $\Omega_m h^2$, $H(0.35)\, r_s(z_d)$, $r_s(z_d)\, /\, D_A(0.35)$, and $A(0.35)$. The diagonal panels represent the marginalized probabilities.

28

	mean	σ	input value
$D_V(0.35)(\text{Mpc})$	1349	69	1356
$\Omega_m h^2$	0.120	0.015	0.1225
$r_s(z_d)/D_V(0.35)$	0.1205	0.0059	0.1175
$A(0.35)$	0.441	0.026	0.452

Table 3.5: The mean, standard deviation, and the 68% C.L. bounds of $\{D_V(0.35), \Omega_m h^2,$ $r_s(z_d)/D_V(0.35), A(0.35)\}$ from the LRGfull mock catalogs of the LasDamas simulations. Our measurements are consistent with the input values within 1σ.

Table 3.5 shows our measurements of $\{D_V(0.35), \Omega_m h^2, r_s(z_d)/D_V(0.35), A(0.35)\}$ from the LasDamas mock catalogs of the SDSS LRG sample. These are consistent with the input parameters, establishing the validity of our method.

3.3 Systematic Tests

Table. 3.6 shows the systematic tests that we have done varying key assumptions made in our analysis. These include the range of scales used to calculate the correlation function, the nonlinear damping scale, an overall shift in the measured correlation function due to a systematic error.

We vary the effective redshift (from $z_{eff} = 0.33$ to $z_{eff} = 0.35$) used to calculate the theoretical model. We rescale the results to $z = 0.35$ for comparison and find that the results are insensitive to the effective redshift.

We also test the sensitivity of our results to the nonlinear damping scale, $k_\star$. Although $k_\star$ can be predicted accurately in the real space (Crocce & Scoccimarro, 2006; Matsubara, 2007), in the redshift space, it would also depend on the redshift distortions which cannot be well determined from the spherically-averaged correlation function. In table. 3.6, one can tell that the results are not sensitive to $k_\star$.

In principle, the range of scales chosen for the analysis should be as large as possible, in order to derive the tightest constraints. However, we do not use the small scales ($s < 40\ h^{-1}\text{Mpc}$), where the scale dependence of redshift distortion and galaxy bias are not negligible and cannot be accurately determined at present. According to Fig. 5 in

Eisenstein et al. (2005), these effects are negligible at $s > 40$ h^{-1}Mpc. We vary the minimum scales used and find that the $r_s(z_d)/D_V(0.35)$ is insensitive to it but $\Omega_m h^2$ is not. This is one of the reasons we recommend to use $r_s(z_d)/D_V(0.35)$ but not $\Omega_m h^2$ from this paper.

On larger scales ($s > 130$ h^{-1}Mpc), the observed correlation is significantly higher than expected in conventional models of galaxy clustering. This high tail problem was reported in previous work, see, e.g., Eisenstein et al. (2005), Hutsi (2005), and Sanchez et al. (2009). They found that the observed correlation function could be fitted better by lowering all the data points by a constant. In other words, they assumed a constant shift from some systematic error. Although this systematic error is unknown, we could minimize its effect by using smaller scale. The reason is that the correlation function has larger value at smaller scale so that the results are less sensitive to the shift. We choose $s = 120h^{-1}Mpc$ as our boundary for the large scale and show that the results are insensitive to the constant shift by lowering down the data points of the observed correlation function by 0.002. We find that $\Omega_m h^2$ varies by 1σ and $r_s/D_V(0.35)$ only varies by 0.2σ. Therefore, our measurement of $r_s/D_V(0.35)$ is robust to the systematic shift. This is another reason we recommend the use of the measured $r_s(z_d)/D_V(0.35)$, but not $\Omega_m h^2$, from this paper.

	$D_V(0.35)$(Mpc)	$\Omega_m h^2$	$r_s(z_d)/D_V(0.35)$	$A(0.35)$
fiducial model	1428^{+74}_{-73}	0.105 ± 0.016	$0.1143^{+0.0029}_{-0.0031}$	0.439 ± 0.02
$z_{eff} = 0.35$	1427^{+72}_{-73}	$0.105^{+0.016}_{-0.015}$	$0.1144^{+0.0030}_{-0.0031}$	0.439 ± 0.02
$k_\star = 0.11$	1426^{+73}_{-72}	0.106 ± 0.015	$0.1144^{+0.0030}_{-0.0031}$	0.439 ± 0.02
s=20-120	1398^{+64}_{-62}	0.116 ± 0.012	0.1139 ± 0.0028	0.453 ± 0.015
s=60-120	1418^{+94}_{-93}	0.108 ± 0.025	$0.1149^{+0.0030}_{-0.0033}$	0.438 ± 0.03
s=40-100	1448^{+96}_{-89}	$0.114^{+0.018}_{-0.019}$	$0.111^{+0.0050}_{-0.0058}$	$0.463^{+0.033}_{-0.032}$
s=40-140	1393^{+90}_{-87}	0.110 ± 0.018	$0.1164^{+0.0040}_{-0.0047}$	$0.437^{+0.025}_{-0.023}$
shift = 0.002	1388^{+80}_{-77}	0.122 ± 0.020	$0.1136^{+0.0032}_{-0.0035}$	0.459 ± 0.023

Table 3.6: This table shows the systematic tests with the scale range, the fiducial model used, the effective redshift, the damping factor, and the shift from a systematic error. The fiducial results is obtained by assuming ΛCDM model with $\Omega_m = 0.25$ as fiducial model considering the scale range ($s = 40 - 120$ h^{-1}Mpc), using the effective redshift ($z_{eff} = 0.33$)), and the damping factor, $k_\star$, marginalized over with a flat prior ($0.09 < k_\star < 0.13$ hMpc^{-1}). The other results are calculated with only one quantity different from the fiducial one. $n_s = 0.963$ and $\Omega_b h^2 = 0.02258$ are marginalized with the same flat priors ($\pm 7\sigma_{WMAP7}$) in this paper.

Chapter 4 Measurements from Two-Dimensional Two-Point Correlation Function

In previous chapter, we presented the method to obtain dark energy and cosmological model constraints from the spherically-averaged 2PCF, without assuming a dark energy model or a flat Universe. We demonstrated the feasibility of extracting $H(z)$ and $D_A(z)$ by scaling the spherically-averaged 2PCF (which leads to highly correlated measurements). In this chapter, we present the method to obtain measurements of $H(z)$ and $D_A(z)$ through using the two-dimensional two-point correlation function.

4.1   Methodology

4.1.1   Measuring the Two-Dimensional Two-Point Correlation Function

We convert the measured redshifts of galaxies to comoving distances by assuming a fiducial model, ΛCDM with $\Omega_m = 0.25$. We use the two-point correlation function estimator given by Landy & Szalay (1993):

$$\xi(\sigma, \pi) = \frac{DD(\sigma, \pi) - 2DR(\sigma, \pi) + RR(\sigma, \pi)}{RR(\sigma, \pi)}, \tag{4.1}$$

where π is the separation along the light of sight (LOS), σ is the separation in the plane of the sky, DD, DR, and RR represent the normalized data-data, data-random, and random-random pair counts respectively in a distance range. The LOS is defined as the direction from the observer to the center of a pair. The bin size we use in this study is $10\,h^{-1}\mathrm{Mpc} \times 10\,h^{-1}\mathrm{Mpc}$. While calculating the pair counts, we assign each data point a radial weight of $1/[1 + n(z) \cdot P_w]$, where $n(z)$ is the radial selection function and $P_w = 4 \cdot 10^4 \ h^{-3}\mathrm{Mpc}^3$ as in Eisenstein et al. (2005).

4.1.2 Theoretical Two-Dimensional Two-Point Correlation Function

In the linear regime (i.e., large scales) and adopting the small-angle approximation (which is valid on scales of interest), the 2D correlation function in the redshift space can be written as (Kaiser, 1987; Hamilton, 1992)

$$\xi^\star(\sigma, \pi) = \xi_0(s)P_0(\mu) + \xi_2(s)P_2(\mu) + \xi_4(s)P_4(\mu), \tag{4.2}$$

where $s = \sqrt{\sigma^2 + \pi^2}$, μ is the cosine of the angle between $\mathbf{s} = (\sigma, \pi)$ and the LOS, and P_l are Legendre polynomials. The multipoles of ξ are defined as

$$\xi_0(r) = \left(1 + \frac{2\beta}{3} + \frac{\beta^2}{5}\right)\xi(r), \tag{4.3}$$

$$\xi_2(r) = \left(\frac{4\beta}{3} + \frac{4\beta^2}{7}\right)[\xi(r) - \bar{\xi}(r)], \tag{4.4}$$

$$\xi_4(r) = \frac{8\beta^2}{35}\left[\xi(r) + \frac{5}{2}\bar{\xi}(r) - \frac{7}{2}\bar{\bar{\xi}}(r)\right], \tag{4.5}$$

where $\xi(r)$ is the correlation function obtained from Eq. 3.6, β is the redshift space distortion parameter and

$$\bar{\xi}(r) = \frac{3}{r^3}\int_0^r \xi(r')r'^2 dr', \tag{4.6}$$

$$\bar{\bar{\xi}}(r) = \frac{5}{r^5}\int_0^r \xi(r')r'^4 dr'. \tag{4.7}$$

Next, we convolve the 2D correlation function with the distribution function of random pairwise velocities, $f(v)$, to obtain the final model $\xi(\sigma, \pi)$ (Peebles, 1980)

$$\xi(\sigma, \pi) = \int_{-\infty}^{\infty} \xi^\star\left(\sigma, \pi - \frac{v}{H(z)a(z)}\right) f(v)dv, \tag{4.8}$$

where the random motions are represented by an exponential form (Ratcliffe et al., 1998; Landy, 2002)

$$f(v) = \frac{1}{\sigma_v \sqrt{2}} \exp\left(-\frac{\sqrt{2}|v|}{\sigma_v}\right), \tag{4.9}$$

where σ_v is the pairwise peculiar velocity dispersion.

The parameter set we use to compute the theoretical correlation function is $\{H(z), D_A(z), \beta, \Omega_m h^2, \Omega_b h^2, n_s, \sigma_v, k_\star\}$, where Ω_m and Ω_b are the density fractions of matter and baryons, n_s is the power law index of the primordial matter power spectrum, and h is the dimensionless Hubble constant ($H_0 = 100h$ km s^{-1}Mpc^{-1}). We set $h = 0.7$ while calculating the non-linear power spectra. On the scales we use for comparison with data, the theoretical correlation function only depends on cosmic curvature and dark energy through parameters $H(z)$ and $D_A(z)$, assuming that dark energy perturbations are unimportant (valid in simplest dark energy models). Thus we are able to extract constraints from data that are independent of a dark energy model and cosmic curvature.

Fig.4.1(a) shows the 2D 2PCF measured from SDSS LRGs compared with a theoretical model. The measured 2D 2PCF of the SDSS LRGs has been smoothed by a Gaussian filter with rms variance of $2h^{-1}$Mpc to illustrate the comparison of data with model in this figure, as the unsmoothed data are very noisy. Smoothing is *not* used in our likelihood analysis to avoid possibly introducing systematic biases. Fig. 4.1(b) shows the 2D 2PCF measured from a single LasDamas SDSS LRG mock catalog for comparison. The similarity between the data and the mock in the range of scales we used (indicated by the shaded disk) is apparent.

Fig.4.2 shows the averaged 2D 2PCF measured from the LasDamas mock catalogs compared with a theoretical model. The contour levels are apparent in the measured 2D 2PCF even though no smoothing is used; this is due to the reduction of shot noise achieved by averaging over 160 mock catalogs. Clearly, our 2D theoretical model provides a reasonable fit to data on intermediate (and quasi-linear) scales. The deviations on smaller scales may be due to the simplicity of the peculiar velocity model we have used.

We do not use the smaller scales ($s < 40\ h^{-1}\mathrm{Mpc}$), where the scale dependence of redshift distortion and galaxy bias are not negligible and cannot be accurately determined at present. According to Fig. 5 in Eisenstein et al. (2005) and Fig. 4 in Blake et al. (2011), these effects are negligible at $s > 40\ h^{-1}\mathrm{Mpc}$. On large scales, data become very noisy as sample variance dominates. For these reasons, we will only use the scale range of $s = 40 - 120\ h^{-1}\mathrm{Mpc}$ in our analysis. We do not consider wide-angle effects, since they have been shown to be small on the length scales of interest here (Samushia et al. , 2011). Since including a larger range of scales gives more stringent constraints, our choice of $s = 40 - 120\ h^{-1}\mathrm{Mpc}$ represents a conservative cut in data to reduce contamination by systematic uncertainties.

4.1.3 Likelihood

The likelihood is taken to be proportional to $\exp(-\chi^2/2)$ (Press et al., 1992), with χ^2 given by

$$\chi^2 \equiv \sum_{i,j=1}^{N_{bins}} \left[\xi_{th}(\mathbf{s}_i) - \xi_{obs}(\mathbf{s}_i)\right] C_{ij}^{-1} \left[\xi_{th}(\mathbf{s}_j) - \xi_{obs}(\mathbf{s}_j)\right] \tag{4.10}$$

where N_{bins} is the number of bins used, $\mathbf{s}_m = (\sigma_m, \pi_m)$, ξ_{th} is the theoretical correlation function, and ξ_{obs} is the observed correlation function. Note that $\xi_{th}(\mathbf{s}_i)$ depends on $\{H(z), D_A(z), \beta, \Omega_m h^2, \Omega_b h^2, n_s, \sigma_v, k_\star\}$.

Again, let us define T as the operator converting the measured correlation function from the fiducial model to another model, i.e.,

$$\xi_{obs}(\mathbf{s}) = T(\xi_{obs}^{fid}(\mathbf{s})), \tag{4.11}$$

where $\xi_{obs}^{fid}(\mathbf{s})$ is the observed correlation function assuming the fiducial model. This
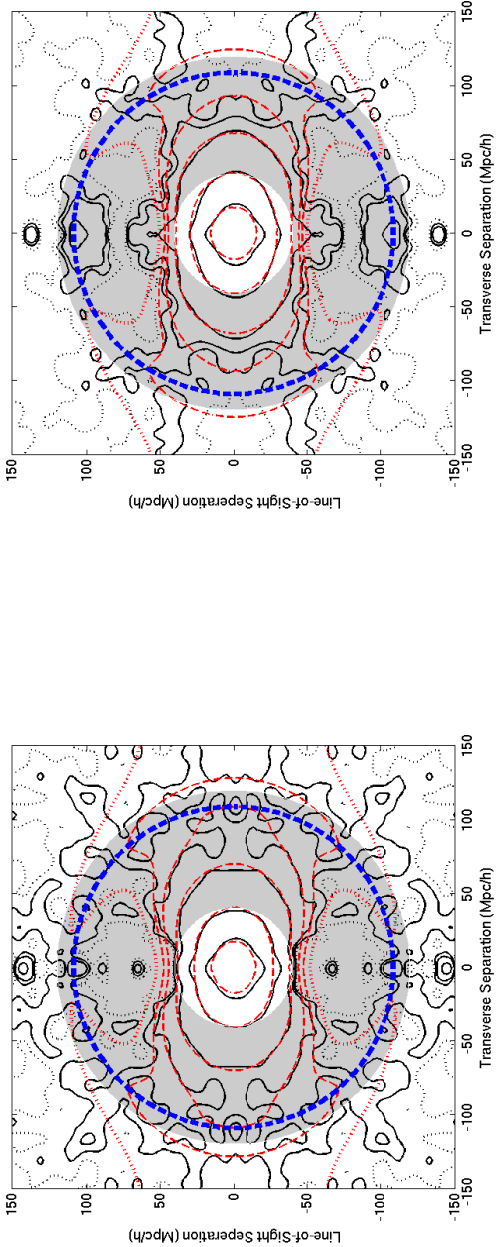
(a) 2D 2PCF from SDSS LRGfull sample

(b) 2D 2PCF from single mock catalog

Figure 4.1: 4.1(a) The two-dimensional two-point correlation function (2D 2PCF) measured from SDSS DR7 LRGs in a redshift range $0.16 < z < 0.44$ (solid black contours), compared to a theoretical correlation function with parameters close to the best fit values in the likelihood analysis (dashed red contours). The theoretical model has $H(z = 0.35) = 81.8 \, \mathrm{km \, s^{-1} \, Mpc^{-1}}$, $D_A(z = 0.35) = 1042 \, \mathrm{Mpc}$, $\beta = 0.35$, $\Omega_m h^2 = 0.117$, $\Omega_b h^2 = 0.022$, $n_s = 0.96$, $\sigma_v = 300 \mathrm{km \, s^{-1}}$, and $k_\star = 0.11$. 4.1(b) The 2D 2PCF measured from a single mock catalog, compared to a theoretical model with the input parameters of the LasDamas simulations and $\{\beta, \sigma_v, k_\star\}$ are set to $\{0.35, 300 \mathrm{km \, s^{-1}}, 0.11 h \mathrm{Mpc^{-1}}\}$ (dashed red contours). In both figures, the shaded disk indicates the scale range considered ($s = 40 - 120 \, h^{-1}\mathrm{Mpc}$) in this study. The thick dashed blue circle denotes the baryon acoustic oscillation scale. Both the observed and mock data of the 2D 2PCF has been smoothed by a Gaussian filter with rms variance of $2h^{-1}\mathrm{Mpc}$ for illustration in these figures only; smoothing is not used in our likelihood analysis. The contour levels are $\xi = 0.5, \, 0.1, \, 0.025, \, 0.01, \, 0.005, \, 0$. The $\xi = 0$ contours are denoted with dotted lines for clarity.

36
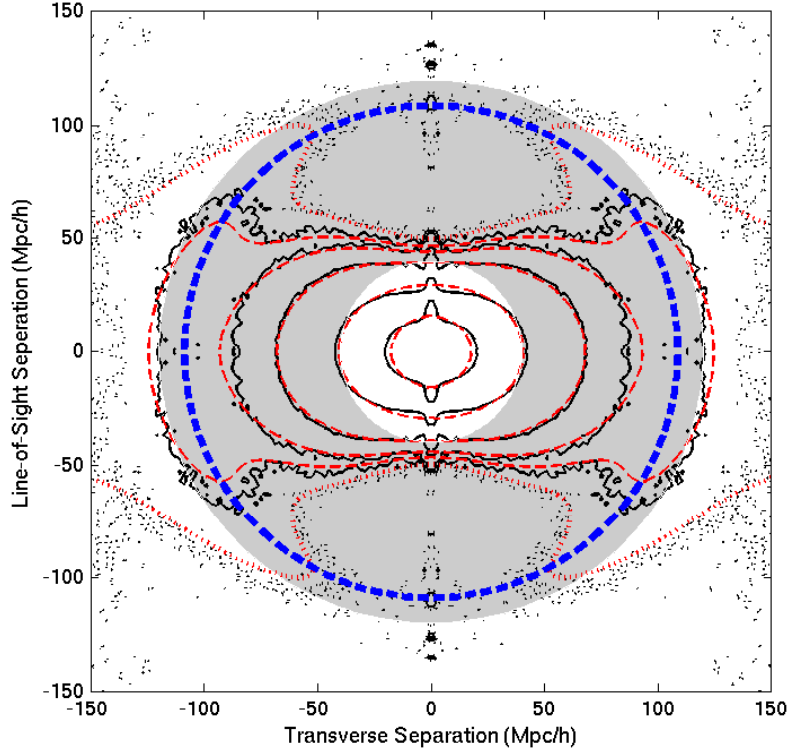
Figure 4.2: The average two-dimensional two-point correlation function (2D 2PCF) measured from 160 LasDamas SDSS LRGfull mock catalogs (solid black contours), compared to a theoretical model with the input parameters of the LasDamas simulations and $\{\beta, \sigma_v, k_\star\}$ are set to $\{0.35, 300\text{km s}^{-1}, 0.11h\text{Mpc}^{-1}\}$ (dashed red contours). The gray area is the scale range considered ($s = 40 - 120 \ h^{-1}\text{Mpc}$) in this study. The thick dashed blue circle denotes the baryon acoustic oscillation scale. The contour levels are apparent in the 2D 2PCF measured from mock catalogs, even though no smoothing is used. The contour levels are $\xi = 0.5, 0.1, 0.025, 0.01, 0.005, 0$. The $\xi = 0$ contours are denoted with dotted lines for clarity.

37

allows us to rewrite χ^2 as

$$\chi^2 \equiv \sum_{i,j=1}^{N_{bins}} \left\{ T^{-1}\left[\xi_{th}(\mathbf{s}_i)\right] - \xi_{obs}^{fid}(\mathbf{s}_i) \right\} C_{fid,ij}^{-1} \cdot$$
$$\cdot \left\{ T^{-1}\left[\xi_{th}(\mathbf{s}_j)\right] - \xi_{obs}^{fid}(\mathbf{s}_j) \right\}, \tag{4.12}$$

where we have used Eqs.(3.9) and (4.11).

To find the operator T, note that the fiducial model is only used in converting redshifts into distances for the galaxies in our data sample. In the analysis of galaxy clustering, we only need the separation of a galaxy pair, and not the absolute distances to the galaxies. For a thin redshift shell, we can convert the separation of one pair of galaxies from the fiducial model to another model by performing the scaling (see, e.g., Seo & Eisenstein (2003))

$$(\sigma', \pi') = \left(\frac{D_A(z)}{D_A^{fid}(z)}\sigma, \frac{H^{fid}(z)}{H(z)}\pi \right). \tag{4.13}$$

Therefore, we can convert the measured 2D correlation function from some model to the fiducial model as follows:

$$\xi_{obs}^{fid}(\sigma, \pi) = T^{-1}(\xi_{obs}(\sigma, \pi))$$
$$= \xi_{obs}\left(\frac{D_A(z)}{D_A^{fid}(z)}\sigma, \frac{H^{fid}(z)}{H(z)}\pi \right). \tag{4.14}$$

This mapping defines the operator T.

We now apply the inverse operation to the theoretical correlation function:

$$T^{-1}(\xi_{th}(\sigma, \pi)) = \xi_{th}\left(\frac{D_A(z)}{D_A^{fid}(z)}\sigma, \frac{H^{fid}(z)}{H(z)}\pi \right). \tag{4.15}$$

χ^2 can be calculated by substituting eq. (4.15) into eq. (4.12).

38

4.1.4 Markov Chain Monte-Carlo Likelihood Analysis

We use CosmoMC in a Markov Chain Monte-Carlo likelihood analysis (Lewis & Bridle, 2002). The parameter space that we explore spans the parameter set of $\{H(0.35),$ $D_A(0.35),\ \Omega_m h^2,\ \beta,\ \Omega_b h^2,\ n_s,\ \sigma_v,\ k_\star\}$. Only $\{H(0.35), D_A(0.35), \Omega_m h^2\}$ are well constrained using SDSS LRGs alone. We marginalize over the other parameters, $\{\beta,\ \Omega_b h^2,$ $n_s,\ \sigma_v,\ k_\star\}$, with the flat priors, $\{(0.1, 0.6),\ (0.01859, 0.02657),\ (0.865, 1.059),\ (0, 500)\text{km}$ $\text{s}^{-1},\ (0.09,\ 0.13)h\text{Mpc}^{-1}\}$, where the flat priors of $\Omega_b h^2$ and n_s are centered on the measurements from WMAP7 and has width of $\pm 7\sigma_{WMAP}$ (with σ_{WMAP} from Komatsu et al. (2010)). These priors are wide enough to ensure that CMB constraints are not double counted when our results are combined with CMB data (Chuang, Wang, & Hemantha, 2010). We also marginalize over the amplitude of the galaxy correlation function, effectively marginalizing over a linear galaxy bias.

4.2 Results

We now present the model independent measurements of the parameters $\{\ H(0.35),$ $D_A(0.35),\ \Omega_m h^2\}$, obtained by using the method described in previous sections. We also present the derived parameters including $H(0.35)\,r_s(z_d)$, $r_s(z_d)/D_A(0.35)$, $r_s(z_d)\ /$ $D_V(0.35)$, and $A(0.35)$, where

$$D_V(z) \equiv \left[(1+z)^2 D_A^2 \frac{cz}{H(z)}\right]^{\frac{1}{3}} \tag{4.16}$$

We recommend using $\{H(0.35)\,r_s(z_d),\ r_s(z_d)/D_A(0.35)\}$ instead of $\{H(0.35),\ D_A(0.35),$ $\Omega_m h^2\}$ because they are more robust measurements from this study (see Sec. 4.3 for more detail). We apply our method to the 2D 2PCF of the LasDamas mock catalogs and find that our measurements are consistent with the input parameters of the simulations.
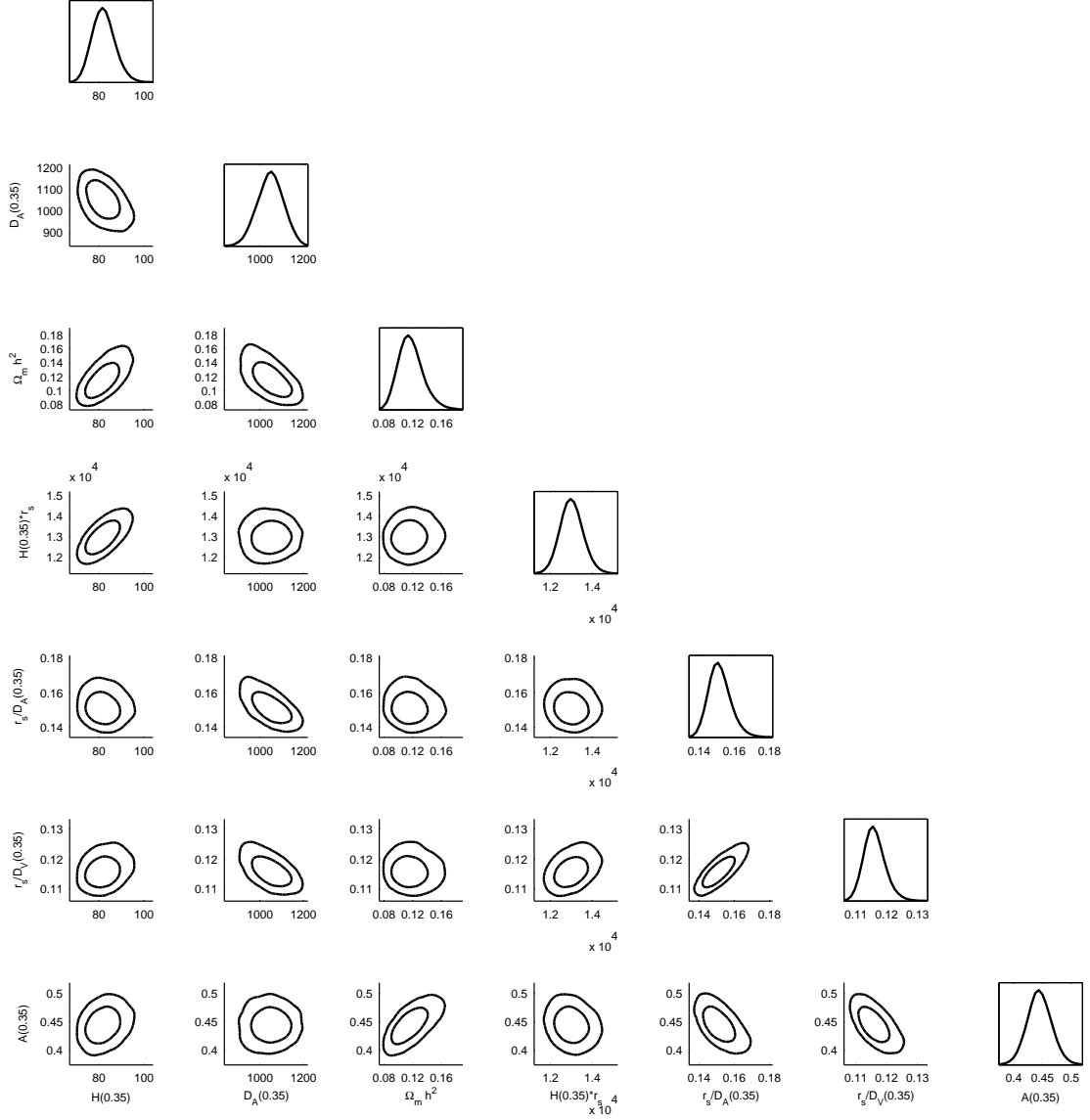
Figure 4.3: 2D marginalized contours (68% and 95% C.L.) for $\{H(0.35),\ D_A(0.35),\ \Omega_m h^2,\ H(0.35)\,r_s(z_d),\ r_s(z_d)/D_A(0.35),\ r_s(z_d)/D_V(0.35),\ A(0.35)\}$. The diagonal panels represent the marginalized probabilities. The unit of H is $\mathrm{km\,s^{-1}\,Mpc^{-1}}$. The unit of D_A, D_V, and $r_s(z_d)$ is Mpc.

	mean	σ	lower	upper
$H(0.35)$	82.1	5.0	77.2	86.9
$D_A(0.35)$	1048	58	990	1107
$\Omega_m h^2$	0.118	0.017	0.101	0.133
$H(0.35)\,r_s(z_d)$	**13020**	**530**	**12500**	**13530**
$r_s(z_d)/D_A(0.35)$	**0.1518**	**0.0062**	**0.1460**	**0.1576**
$r_s(z_d)/D_V(0.35)$	0.1161	0.0034	0.1129	0.1193
$A(0.35)$	0.445	0.021	0.425	0.465

Table 4.1: The mean, standard deviation, and the 68% C.L. bounds of $\{H(0.35),\ D_A(0.35),\ \Omega_m h^2,\ H(0.35)\,r_s(z_d),\ r_s(z_d)/D_A(0.35), r_s(z_d)/D_V(0.35), A(0.35)\}$ from SDSS DR7 LRGs. We recommend using $H(0.35)\,r_s(z_d)$ and $r_s(z_d)\ /\ D_A(0.35)$ for further analysis. The unit of H is $\mathrm{km\,s^{-1}\,Mpc^{-1}}$. The unit of D_A, D_V, and $r_s(z_d)$ is Mpc.

	$H(0.35)$	$D_A(0.35)$	$\Omega_m h^2$	$H(0.35)\,r_s(z_d)$	$r_s(z_d)/D_A(0.35)$	$r_s(z_d)/D_V(0.35)$	$A(0.35)$
$H(0.35)$	1	-0.4809	0.7088	0.7297	-0.0806	0.2641	0.2618
$D_A(0.35)$	-0.4809	1	-0.6339	-0.0065	-0.6725	-0.6175	0.0379
$\Omega_m h^2$	0.7088	-0.6339	1	0.0867	-0.0865	-0.0395	0.7042
$H(0.35)\,r_s(z_d)$	0.7297	-0.0065	0.0867	1	**-0.0584**	0.4099	-0.1934
$r_s(z_d)/D_A(0.35)$	-0.0806	-0.6725	-0.0865	**-0.0584**	1	0.8864	-0.6417
$r_s(z_d)/D_V(0.35)$	0.2641	-0.6175	-0.0395	0.4099	0.8864	1	-0.6768
$A(0.35)$	0.2618	0.0379	0.7042	-0.1934	-0.6417	-0.6768	1

Table 4.2: Normalized covariance matrix of the measured and derived parameters, $\{H(0.35),\ D_A(0.35),\ \Omega_m h^2,\ H(0.35)\,r_s(z_d),$ $r_s(z_d)/D_A(0.35),\ r_s(z_d)\ /\ D_V(0.35),\ A(0.35)\}$.

4.2.1 Constraints on $H(0.35)$ and $D_A(0.35)$ Independent of a Dark Energy Model

Fig. 4.3 shows one and two-dimensional marginalized contours of the parameters, $\{H(0.35),\, D_A(0.35),\, \Omega_m h^2,\, H(0.35)\, r_s(z_d),\, r_s(z_d)/D_A(0.35),\, r_s(z_d)/D_V(0.35),\, A(0.35)\}$, derived in an MCMC likelihood analysis from the measured 2D 2PCF of the SDSS LRG sample. Table 4.1 lists the mean, rms variance, and 68% confidence level limits of these parameters. Table 4.2 gives the normalized covariance matrix for this parameter set. These are independent of a dark energy model, and obtained without assuming a flat Universe.

The constraints on $\{H(0.35),\, D_A(0.35),\, \Omega_m h^2\}$, $\{H(0.35)\, r_s(z_d),\, r_s(z_d)/D_A(0.35)\}$, $r_s(z_d)/D_V(0.35)$, or $A(0.35)\}$, as summarized in Tables 4.1 and 4.2, can be used to combined with any other cosmological data set to constrain dark energy and the cosmological model. We recommend using only $\{H(0.35)\, r_s(z_d), r_s(z_d)/D_A(0.35)\}$ since they have tighter constraints than $\{H(0.35), D_A(0.35)\}$ and are robust in the systematic tests we have carried out (see Sec. 4.3). In addition, $H(0.35)\, r_s(z_d)$ and $r_s(z_d)/D_A(0.35)$ are basically independent to $\Omega_m h^2$ which might not a robust measurement in this study (see Sec. 4.3).

The bestfit model from the MCMC likelihood analysis has $\chi^2 = 112$ for 99 bins of data used (in the scale range of $40\, h^{-1}\mathrm{Mpc} < s < 120\, h^{-1}\mathrm{Mpc}$ for $10\, h^{-1}\mathrm{Mpc} \times 10\, h^{-1}\mathrm{Mpc}$ bins), for a set of 9 parameters (including the overall amplitude of the correlation function) and the χ^2 per degree of freedom (χ^2/d.o.f.) is 1.24.

4.2.2 Validation Using Mock Catalogs

In order to validate our method, we have applied it to the 2D 2PCF of 80 LasDamas mock catalogs (which are indexed with 01a-40a and 01b-40b). Again, we apply the flat and wide priors ($\pm 7\sigma_{WMAP7}$) on $\Omega_b h^2$ and n_s, centered on the input values of the simulation ($\Omega_b h^2 = 0.0196$ and $n_s = 1$).

	mean	σ	input value
$H(0.35)$	81.1	4.1	81.79
$D_A(0.35)$	1008	56	1032.8
$\Omega_m h^2$	0.121	0.013	0.1225
$H(0.35)\,r_s(z_d)$	13030	610	13030
$r_s(z_d)/D_A(0.35)$	0.1606	0.0078	0.1543
$r_s(z_d)/D_V(0.35)$	0.1205	0.0046	0.1175
$A(0.35)$	0.440	0.019	0.452

Table 4.3: The mean, standard deviation, and the 68% C.L. bounds of $\{H(0.35),$ $D_A(0.35),$ $\Omega_m h^2,$ $H(0.35)\,r_s(z_d),$ $r_s(z_d)/D_A(0.35),$ $r_s(z_d)/D_V(0.35),$ $A(0.35)\}$ from the 2D 2PCF of 80 LasDamas mock catalogs (which are indexed with 01a-40a and 01b-40b). Our measurements are consistent with the input values within 1σ, where each σ is computed from the 80 means measured from the 80 mock catalogs. The unit of H is $\mathrm{km\,s^{-1}\,Mpc^{-1}}$. The unit of D_A, D_V, and $r_s(z_d)$ is Mpc.

Table 4.3 shows the means and standard deviations of our measurements of $\{H(0.35),$ $D_A(0.35),$ $\Omega_m h^2,$ $H(0.35)\,r_s(z_d),$ $r_s(z_d)/D_A(0.35),$ $r_s(z_d)/D_V(0.35),$ $A(0.35)\}$ from the LasDamas mock catalogs of the SDSS LRG sample. These are consistent with the input parameters, establishing the validity of our method.

4.3 Systematic Tests

Table. 4.4 shows the systematic tests that we have carried out varying key assumptions made in our analysis. These include the range of scales used to calculate the correlation function, the nonlinear damping factor, the bin size, and an overall shift in the measured correlation function due to a systematic error.

First, we fix the nonlinear damping factor, $k_\star = 0.11$, and find the results are basically the same. To speed up the computation, we fix $k_\star$ for the rest of the tests.

In this study, we marginalize over β with a wide flat prior (0.1 to 0.6) since our method is not sensitive to β. We test fixing the value of β to 0.35, which is close to the measurement from previous work with similar data but using different method (Cabre & Gaztanaga, 2008), and find that our measurements of $H(0.35)\,r_s(z_d)$ and $r_s(z_d)/D_A(0.35)$ change by less than 1% compared to that of marginalizing over β.

We vary the range of the scale and find that $H(0.35) \, r_s(z_d)$ and $r_s(z_d)/D_A(0.35)$ are insensitive to it. However, $\Omega_m h^2$ is sensitive to the minimum scale chosen which could imply that the scale dependent bias or redshift distortion is distorting larger scale than we have expected. Therefore, we do not recommend to use $\Omega_m h^2$ from this study. In the case of $s = 40 - 130 h^{-1}\mathrm{Mpc}$, $r_s(z_d)/D_A(0.35)$ is different from the fiducial result with about 2σ, which is likely due to systematic errors responsible for the anomalously high tail in the spherically-averaged correlation function (see Fig. 3.1) on large scales.

We vary the bin size to $8h^{-1}\mathrm{Mpc}\times 8h^{-1}\mathrm{Mpc}$ and find $\chi^2/\mathrm{d.o.f.}= 1.72$, which can be explained by the increase in the noise level with the increased number of bins. The number of the mock catalogs used to construct the covariance matrix is 160 and the number of bins used with bin size $= 8h^{-1}\mathrm{Mpc}\times 8h^{-1}\mathrm{Mpc}$ is 159. One can expect the covariance matrix would be too noisy to give reasonable results.

We also show that the results are insensitive to the constant shift by lowering down the data points of the observed correlation function by 0.001 and 0.002.

	$H(0.35)$	$D_A(0.35)$	$\Omega_m h^2$	$H(0.35)\,r_s(z_d)$	$r_s(z_d)/D_A(0.35)$	$r_s(z_d)/D_V(0.35)$	$A(0.35)$	χ^2/d.o.f.
fiducial result	$82.1^{+4.8}_{-4.9}$	1048^{+60}_{-58}	0.118 ± 0.016	13020^{+510}_{-510}	0.1518 ± 0.0059	0.1161 ± 0.0033	0.445 ± 0.020	1.24
$k_\star = 0.11$	$81.9^{+4.9}_{-5.0}$	1049 ± 59	0.117 ± 0.017	13020^{+520}_{-510}	$0.1519^{+0.0057}_{-0.0059}$	$0.1162^{+0.0033}_{-0.0034}$	0.444 ± 0.020	1.24
$\beta = 0.35$	83.9 ± 5.6	1008 ± 53	0.132 ± 0.020	12897 ± 500	$0.1531^{+0.0056}_{-0.0057}$	$0.1164^{+0.0032}_{-0.0033}$	0.456 ± 0.021	1.25
$30 < s < 120, k_\star = 0.11$	$83.4^{+4.5}_{-4.7}$	1038^{+52}_{-51}	$0.120^{+0.013}_{-0.014}$	13120^{+560}_{-550}	$0.1520^{+0.0052}_{-0.0053}$	0.1166 ± 0.0032	0.446 ± 0.016	1.24
$50 < s < 120, k_\star = 0.11$	$83.9^{+5.5}_{-5.4}$	1014^{+65}_{-65}	$0.133^{+0.024}_{-0.023}$	12880 ± 590	$0.1521^{+0.0061}_{-0.0062}$	$0.1158^{+0.0032}_{-0.0033}$	0.459 ± 0.024	1.06
$40 < s < 110, k_\star = 0.11$	80.6 ± 5.1	1087^{+59}_{-60}	0.115 ± 0.016	12880^{+570}_{-560}	$0.1477^{+0.0057}_{-0.0059}$	0.1136 ± 0.0035	$0.454^{+0.022}_{-0.021}$	1.09
$40 < s < 130, k_\star = 0.11$	$84.8^{+6.4}_{-6.3}$	987^{+61}_{-60}	0.115 ± 0.016	13540^{+780}_{-780}	$0.1624^{+0.0068}_{-0.0070}$	$0.1230^{+0.0042}_{-0.0043}$	0.418 ± 0.019	1.31
bin size $= 8h^{-1}$Mpc$\times 8h^{-1}$Mpc	$87.9^{+5.6}_{-6.0}$	1037 ± 60	$0.139^{+0.017}_{-0.018}$	13410^{+700}_{-720}	0.1477 ± 0.0058	$0.1151^{+0.0038}_{-0.0036}$	$0.470^{+0.021}_{-0.020}$	1.72
shift$= 0.001, k_\star = 0.11$	$83.0^{+5.4}_{-5.3}$	1041^{+61}_{-60}	$0.124^{+0.019}_{-0.018}$	13000^{+750}_{-540}	0.1510 ± 0.0060	$0.1157^{+0.0035}_{-0.0034}$	0.453 ± 0.021	1.25
shift$= 0.002, k_\star = 0.11$	$85.2^{+5.4}_{-5.6}$	1024^{+63}_{-65}	$0.135^{+0.021}_{-0.020}$	13060 ± 560	$0.1503^{+0.0062}_{-0.0063}$	$0.1155^{+0.0037}_{-0.0038}$	0.463 ± 0.022	1.24

Table 4.4: This table shows the systematic tests with the damping factor, the scale range, the bin size, and the assumed constant shift from a systematic error ($\xi_{obs}(s) = \xi_{true}(s)+$shift). The fiducial results are obtained by considering the scale range ($40 < s < 120\ h^{-1}$Mpc), the bin size $= 10h^{-1}$Mpc$\times 10h^{-1}$Mpc, and the damping factor, $k_\star$, marginalized over with the a flat prior ($0.09 < k_\star < 0.13\ h$Mpc^{-1}). The other results are calculated with only specified quantities different from the fiducial one. The unit of H is km s^{-1} Mpc^{-1}. The unit of D_A, D_V, and $r_s(z_d)$ is Mpc.

Chapter 5   Constraints on owCDM Model

We now present the cosmological parameter constraints for the owCDM model (non-flat Universe with a constant dark energy equation of state). Table. 5.1 also shows the constraints from cosmological microwave background (WMAP7) and supernova (Union2 compilation) data and their combination with SDSS LRG data. To include the constraints from WMAP7 (Komatsu et al., 2010), we use the constraints on the CMB shift parameters $\{R, l_a\}$ and z_* by Wang, Chuang, & Mukherjee (2011) (see Appendix B). To calculate the constraints from Union2 SNe (Amanullah et al., 2010), we use the add-on code for cosmoMC which can be download from the website of Union2 SNe[1]. For a given model, one could obtain χ^2 for each data set, i.e. χ^2_{CMB} and χ^2_{SN}[2]. To include the constraint we obtained from the spherical-averaged 2PCF, one should add the following term to the χ^2 with

$$\chi^2_{LRG1D} = \left[\frac{r_s(z_d)/D_V(0.35) - 0.1143}{0.0033} \right]^2. \tag{5.1}$$

To include the constraints we obtained from the 2D 2PCF, one should add the following term to the χ^2 with

$$\chi^2_{LRG2D} = \Delta_{LRG2D} \begin{pmatrix} 280900 & -1919 \\ -1919 & 0.00003844 \end{pmatrix} \Delta_{LRG2D} \tag{5.2}$$

where

$$\Delta_{LRG2D} = \begin{pmatrix} H(0.35)r_s(z_d) - 0.13020 \\ r_s(z_d)/D_A(0.35) - 0.1518 \end{pmatrix} \tag{5.3}$$

Combining all three data sets, LRG(2D), CMB, and SNe, and assuming the owCDM model, we find that $\Omega_k = -0.0004 \pm 0.0070$ and $w = -0.996 \pm 0.043$, which is consistent

---

[1]http://supernova.lbl.gov/Union/

[2]While computing χ^2_{SN}, we use the covariance matrix with systematics to obtain more reliable constraints from SNe
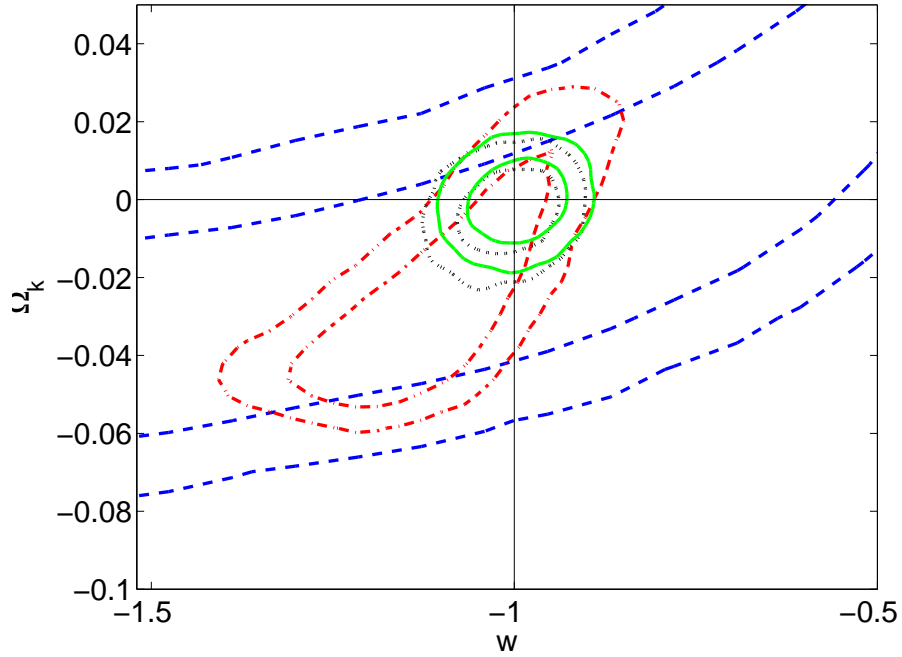
Figure 5.1: 2D marginalized contours for 68% and 95% for w and Ω_k (owCDM model assumed) from WMAP7 (dashed blue), WMAP7+Union2 SN (dash-dotted red), WMAP7+Union2 SN+LRG1D (dotted black), and WMAP7+Union2 SN+LRG2D (solid green). The straight solid black lines indicate that $w = -1$ and $\Omega_k = 0$.

with ΛCDM model (in agreement with previous work, see e.g., Serra et al. 2009; Wang 2009; Mortonson, Hu, & Huterer 2010; Zhao & Zhang 2010). Fig. 5.1 compares the constraints on w and Ω_k in the owCDM model. We can see that the addition of SDSS LRG data significantly tightens the constraints on dark energy and cosmological parameters.

owCDM

	Ω_m	Ω_X	w	H_0	$\Omega_m h^2$	Ω_k
CMB	$0.325^{+0.072}_{-0.077}$	$0.67^{+0.073}_{-0.071}$	$-1.04^{+0.62}_{-0.63}$	$65.7^{+8.2}_{-7.2}$	$0.1356^{+0.0059}_{-0.0060}$	$0.006^{+0.058}_{-0.048}$
CMB+SN	$0.348^{+0.06}_{-0.072}$	$0.676^{+0.052}_{-0.045}$	-1.11 ± 0.11	$63.4^{+6.5}_{-5.8}$	$0.1361^{+0061}_{-0.0060}$	$-0.025^{+0.022}_{-0.019}$
CMB+SN+LRG1D	$0.279^{+0.018}_{-0.019}$	0.725 ± 0.018	$-1.01^{+0.046}_{-0.045}$	69.9 ± 2.3	$0.1357^{+0.0061}_{-0.0059}$	$-0.0032^{+0.0074}_{-0.0072}$
CMB+SN+LRG2D	0.269 ± 0.018	0.731 ± 0.017	-0.996 ± 0.043	71 ± 2.4	$0.1356^{+0.0061}_{-0.0062}$	-0.0004 ± 0.0070

Table 5.1: Constraints of the cosmological parameters from various data combinations with owCDM model assumed, where LRG1D is using the measurement from the spherically-averaged 2PCF(eq. 5.1) and LRG2D is using the measurements from 2D 2PCF(eq. 5.2). There are two inferred parameters, Ω_m and Ω_k, in this table.

Chapter 6   Conclusion

We have presented our first results for the model independent constraints on dark energy from the spherically-averaged correlation function and the two-dimensional correlation function of SDSS DR7 data, using an MCMC likelihood analysis. We find $D_V(0.35) = 1428^{+74}_{-73}$ and $r_s(z_d)/D_V(0.35) = 0.1143 \pm 0.0030$ from the spherically-averaged correlation function. By scaling the spherically-averaged correlation function, we find the Hubble parameter $H(0.35) = 83^{+13}_{-15}$ km s^{-1}Mpc^{-1} and the angular diameter distance $D_A(0.35) = 1089^{+93}_{-87}$ Mpc.

We then generalize the method and find $H(0.35) = 82.1^{+4.8}_{-4.9}$ km s^{-1} Mpc^{-1}, $D_A(0.35) = 1048^{+60}_{-58}$ Mpc from the two-dimensional correlation function. These are the first measurements of $H(z)$ and $D_A(z)$ from galaxy clustering data. Our galaxy clustering measurements of $H(0.35)\, r_s(z_d)$ and $r_s(z_d)/D_A(0.35)$ can be used to combine with CMB and other cosmological data sets to probe dark energy.

We recommend using $H(0.35)\, r_s(z_d)$ and $r_s(z_d)/D_A(0.35)$ measured from the SDSS LRGs for combination with other data sets, since they are tight constraints (4%) that are nearly uncorrelated, and robust with respect to tests of systematic uncertainties. This is as expected, since $H(0.35)\, r_s(z_d)$ and $r_s(z_d)/D_A(0.35)$ correspond to the preferential redshift separation along the line of sight, and the preferential angular separation in the transverse direction respectively; these in turn arise from the BAO in the radial and transverse directions. The measurable preferential redshift and angular separations should be uncorrelated since they are independent degrees of freedom. The presence of the BAO (although only marginally visible in Fig.1) leads to tight and robust constraints on $H(0.35)\, r_s(z_d)$ and $r_s(z_d)/D_A(0.35)$. Since most of the constraining power in our analysis comes from fitting the overall shape of the galaxy correlation function on quasi-linear scales, and not from fitting the BAO peaks, we refer to our measurements as galaxy clustering measurements.

We have validated our method by applying it to the mock catalogs from LasDamas, and finding consistency between our measurements and the input parameters of the LasDamas simulations for samples (see Table 3.5 and 4.3).

Our work has significant implications for future surveys in establishing the feasibility of measuring both $H(z)$ and $D_A(z)$ from galaxy clustering data. In future work, we will optimize our method, and apply it to new observational data as they become available, and to simulated data of planned surveys to derive robust forecasts for dark energy constraints.

Bibliography

Abazajian, K. N., *et al.* [SDSS Collaboration], Astrophys. J. Suppl. **182**, 543 (2009) [arXiv:0812.0649 [astro-ph]].

Amanullah, R., *et al.*, Astrophys. J. **716**, 712 (2010) [arXiv:1004.1711 [astro-ph.CO]].

Bacon DJ, Refregier AR, Ellis RS *MNRAS* 318:625 (2000)

Bennett, C. L., *et al.*, Astrophys. J. Suppl. **148**, 1 (2003)

A. A. Berlind, D. H. Weinberg, Astrophys. J. **575**, 587-616 (2002). [astro-ph/0109001].

Blake, C., Glazebrook, K, 2003, ApJ, 594, 665

Blake, C.; Collister, A.; Bridle, S.; and Lahav, O., Mon. Not. Roy. Astron. Soc. **374**, 1527 (2007) [arXiv:astro-ph/0605303].

Blake, C., et al. 2009, MNRAS, 395, 240

C. Blake *et al.*, arXiv:1105.2862 [astro-ph.CO].

Blanton, M. R., *et al.* [SDSS Collaboration], Astron. J. **129**, 2562 (2005) [arXiv:astro-ph/0410166].

Blanton, M. R.; and Roweis, S., Astron. J. **133**, 734 (2007) [arXiv:astro-ph/0606170].

Cabre, A.; and Gaztanaga, E., arXiv:0807.2460 [astro-ph].

Chuang, C. H.; Wang, Y.; and Hemantha, M. D. P., arXiv:1008.4822 [astro-ph.CO].

C. H. Chuang and Y. Wang, arXiv:1102.2251 [astro-ph.CO].

Cimatti, A.; Robberto, M.; Baugh, C.; Beckwith, S. V. W.; Content, R.; Daddi, E.; De Lucia, G.; Garilli, B.; Guzzo, L.; Kauffmann, G.; Lehnert, M.; Maccagni, D.; Martnez-Sansigre, A.; Pasian, F.; Reid, I. N.; Rosati, P.; Salvaterra, R.; Stiavelli, M.; Wang, Y.; Osorio, M. Zapatero; the SPACE team, Experimental Astronomy, 23, 39 (2009)

Coles, P., and Jones, B., Mon. Not. Roy. Astron. Soc. **248** (1991) 1.

Colless, M., *et al.* [The 2DFGRS Collaboration], Mon. Not. Roy. Astron. Soc. **328**, 1039 (2001) [arXiv:astro-ph/0106498].

Colless, M., *et al.*, arXiv:astro-ph/0306581.

M. Crocce and R. Scoccimarro, Phys. Rev. D **73**, 063520 (2006) [arXiv:astro-ph/0509419].

Eisenstein, D. J.; and Hu, W., Astrophys. J. **496**, 605 (1998) [arXiv:astro-ph/9709112].

Eisenstein, D. J., *et al.* [SDSS Collaboration], Astron. J. **122**, 2267 (2001) [arXiv:astro-ph/0108153].

Eisenstein, D. J., *et al.* [SDSS Collaboration], Astrophys. J. **633**, 560 (2005) [arXiv:astro-ph/0501171].

Eisenstein, D. J.; Seo, H. j.; and White, M. J., Astrophys. J. **664**, 660 (2007) [arXiv:astro-ph/0604361].

Eisenstein, D.J., et al., 2011, arXiv:1101.1529v1 [astro-ph.IM]

Fioc, M.; and Rocca-Volmerange, B., Astron. Astrophys. **326**, 950 (1997) [arXiv:astro-ph/9707017].

Fukugita, M.; Ichikawa, T.; Gunn, J. E.; Doi, M.; Shimasaku, K.; and Schneider, D. P., Astron. J. **111**, 1748 (1996).

E. Gaztanaga, A. Cabre and L. Hui, Mon. Not. Roy. Astron. Soc. **399**, 1663 (2009) [arXiv:0807.3551 [astro-ph]].

Gunn, J. E., *et al.* [SDSS Collaboration], Astron. J. **116**, 3040 (1998) [arXiv:astro-ph/9809085].

Gunn, J. E., *et al.* [SDSS Collaboration], Astron. J. **131**, 2332 (2006) [arXiv:astro-ph/0602326].

Hamilton, A. J. S., 1992, APJL, 385, L5

W. Hu and N. Sugiyama, Astrophys. J. **471**, 542 (1996) [arXiv:astro-ph/9510117].

Hutsi, G., arXiv:astro-ph/0507678.

N. Kaiser, Mon. Not. Roy. Astron. Soc. **227**, 1 (1987).

Kazin, E. A., *et al.*, Astrophys. J. **710**, 1444 (2010) [arXiv:0908.2598 [astro-ph.CO]].

E. A. Kazin, M. R. Blanton, R. Scoccimarro, C. K. McBride and A. A. Berlind, Astrophys. J. **719**, 1032 (2010) [arXiv:1004.2244 [astro-ph.CO]].

Kaiser N, Wilson G, Luppino GA arXiv:astro-ph/0003338 (2000)

Komatsu, E., *et al.*, arXiv:1001.4538 [astro-ph.CO].

Landy, S. D.; and Szalay, A. S., Astrophys. J. **412**, 64 (1993).

S. D. Landy, "The Pairwise Velocity Distribution Function of Galaxies in the LCRS, 2dF, Astrophys. J. **567**, L1 (2002) [arXiv:astro-ph/0202130].

Laureijs, R. et al. 2009, "Euclid Assessment Study Report for the ESA Cosmic Visions", arXiv:0912.0914

Lewis, A.; Challinor, A.; and Lasenby, A., Astrophys. J. **538**, 473 (2000) [arXiv:astro-ph/9911177].

Lewis, A., and Bridle, S., Phys. Rev. D **66**, 103511 (2002) [arXiv:astro-ph/0205436].

McBride, C., et al., in preparation

Martinez, V. J., *et al.*, Astrophys. J. **696**, L93 (2009) [Erratum-ibid. **703**, L184 (2009)] [Astrophys. J. **703**, L184 (2009)] [arXiv:0812.2154 [astro-ph]].

T. Matsubara, Phys. Rev. D **77**, 063530 (2008) [arXiv:0711.2521 [astro-ph]].

Mortonson, M. J.; Hu, W.; Huterer, D., 2010, PRD, 81, 063007

Okumura, T.; Matsubara, T.; Eisenstein, D. J.; Kayo, I.; Hikage, C.; Szalay, A. S.; and Schneider, D. P., Astrophys. J. **676**, 889 (2008) [arXiv:0711.3640 [astro-ph]].

Padmanabhan, N., *et al.* [SDSS Collaboration], Mon. Not. Roy. Astron. Soc. **378**, 852 (2007) [arXiv:astro-ph/0605302].

Peebles, P. J. E. 1980, The Large-Scale Structure of the Universe (Princeton, NJ: Princeton University Press)

Penzias, A. A.; and Wilson, R. W., Astrophys. J. **142**, 419 (1965).

Percival, W. J.; Verde, L.; and Peacock, J. A., Mon. Not. Roy. Astron. Soc. **347**, 645 (2004) [arXiv:astro-ph/0306511].

Percival, W. J.; Cole, S.; Eisenstein, D. J.; Nichol, R. C.; Peacock, J. A.; Pope, A. C.; and Szalay, A. S., Mon. Not. Roy. Astron. Soc. **381**, 1053 (2007) [arXiv:0705.3323 [astro-ph]].

Percival, W. J., *et al.*, Mon. Not. Roy. Astron. Soc. **401**, 2148 (2010) [arXiv:0907.1660 [astro-ph.CO]].

Perlmutter, S., *et al.* [Supernova Cosmology Project Collaboration], Astrophys. J. **517**, 565 (1999) [arXiv:astro-ph/9812133].

Press W.H., Teukolsky S,A., Vetterling W.T., Flannery B.P., 1992, Numerical recipes in C. The art of scientific computing, Second edition, Cambridge: University Press.

Ratcliffe, A., et al., 1998, VizieR Online Data Catalog, 730, 417

Reid, B. A., *et al.*, arXiv:0907.1659 [astro-ph.CO].

Riess, A. G., *et al.* [Supernova Search Team Collaboration], Astron. J. **116**, 1009 (1998) [arXiv:astro-ph/9805201].

L. Samushia, W. J. Percival and A. Raccanelli, arXiv:1102.1014 [astro-ph.CO].

Sanchez, A. G.; Baugh, C. M.; and Angulo, R., Mon. Not. Roy. Astron. Soc. **390**, 1470 (2008) [arXiv:0804.0233 [astro-ph]].

Sanchez, A. G.; Crocce, M.; Cabre, A.; Baugh, C. M.; and Gaztanaga, E., arXiv:0901.2570 [astro-ph].

Saunders, W., *et al.*, Mon. Not. Roy. Astron. Soc. **317**, 55 (2000) [arXiv:astro-ph/0001117].

Seo, H., Eisenstein, D. J., 2003, ApJ, 598, 720

Serra, P.; Cooray, A.; Holz, D. E.; Melchiorri, A.; Pandolfi, S.; Sarkar, D., 2009, PRD, 80, 121302

Smith, R. E., *et al.* [The Virgo Consortium Collaboration], Mon. Not. Roy. Astron. Soc. **341**, 1311 (2003) [arXiv:astro-ph/0207664].

Strauss, M. A., *et al.* [SDSS Collaboration], Astron. J. **124**, 1810 (2002) [arXiv:astro-ph/0206225].

Tegmark, M., *et al.* [SDSS Collaboration], Astrophys. J. **606**, 702 (2004) [arXiv:astro-ph/0310725].

van Waerbeke, L., et al. *Astron. Astrophys* 358:30 (2000)

Wang, Y., 2006, ApJ, 647, 1

Wang, Y.; Mukherjee, P. 2007, Phys.Rev.D, 76, 103533

Wang, Y., 2009, PRD, 80, 123525

Wang, Y., et al., 2010, MNRAS, 409, 737

Wang, Y.; Chuang, C.-H., & Mukherjee, P. 2011, arXiv:1109.3172

Wittman, D. M.; Tyson, J. A.; Kirkmand, D.; Dell'Antonio, I.; Bernstein, G., Nature, 405, 143 (2000)

York, D. G., *et al.* [SDSS Collaboration], Astron. J. **120**, 1579 (2000) [arXiv:astro-ph/0006396].

Zehavi, I., *et al.* [SDSS Collaboration], Astrophys. J. **621**, 22 (2005) [arXiv:astro-ph/0411557].

Zhao, G.-B.; Zhang, X., PRD, 81, 043518

Chapter A LN Mock Catalogs

One convenient way to generate mock galaxy catalogs for calculating covariance matrix is using lognormal random fields which can approximate the present-day non-linear fluctuation field (Coles & Jones, 1991). We create 500 lognormal (LN) density fields (Coles & Jones, 1991; Percival, Verde, & Peacock, 2004) on a 512^3 grid with box length $4096\ h^{-1}$Mpc. We then draw a random Poisson variable with mean given by the selection functions and lognormal field to create the mock catalogs. We follow the steps described in Percival, Verde, & Peacock (2004) except that we don't cut the input power at 0.25 Nyquist frequency because it makes the restored correlation function deviate from the input one. With a input correlation function, $\xi(r)$, the Gaussian field correlation function is obtained by

$$\xi_G(r) = \ln[1 + \xi(r)], \tag{A.1}$$

and this can be Fourier transformed to the power spectrum, $P_G(k)$. A Gaussian density field $\delta_G(r)$ is generated on the grid with this power spectrum, and the corresponding lognormal field is calculated by

$$\delta_{LN}(r) = \exp\left[\delta_G(r) - \frac{\sigma_G^2}{2}\right] - 1, \tag{A.2}$$

where $1 + \delta_{LN}(r)$ is the lognormal density field which is always positive by definition and σ_G^2 is the variance of the Gaussian density field which can be calculated by

$$\sigma_G^2 = \sum_{i,j,l=1}^{N_{grid}} P_G\left[(k_{x_i}^2 + k_{y_j}^2 + k_{z_l}^2)^{\frac{1}{2}}\right], \tag{A.3}$$

where N_{grid} is the number of grid points, $k_{m_n} = \frac{2\pi}{L}\left(n - \frac{N_{grid}}{2}\right)$, L is the box length, and $m = x$, y, or z. Then, the mock catalogs can be constructed by drawing the Poisson random variables with the means given by this lognormal field and the selection function of the galaxy survey.

To compute the correlation function of these mock catalogs, one should create the random data on the same grid as well to cancel out the effect of the finite size of the grid. The input correlation function in this study is the theoretical correlation function with parameters ($\Omega_m = 0.25$, $\Omega_b = 0.04$, $h = 0.7$, $n_s = 1$) which are the same as the input parameters of the LasDamas simulations. We fix $k^\star = 0.11$ and the amplitude is adjusted to fit the averaged correlation function from the LasDamas mock catalogs we use. We are not fitting the observed correlation function because we want to find out is whether the LN mock catalogs could behave as good as LasDamas mock catalogs while estimating the covariance matrix.

Chapter B   CMB Distance Priors

Wang & Mukherjee (2007) showed that CMB shift parameters (l_a, R), together with $\Omega_b h^2$, provide an efficient and intuitive summary of CMB data as far as dark energy constraints are concerned. It is equivalent to replace $\Omega_b h^2$ with z_*, the redshift to the photon-decoupling surface (Wang, 2009).

The CMB shift parameters are defined as (Wang & Mukherjee, 2007):

$$R \equiv \sqrt{\Omega_m H_0^2}\, r(z_*), l_a \equiv \pi r(z_*)/r_s(z_*), \tag{B.1}$$

and $z_\star$ is the redshift to the photon-decoupling surface given by the fitting formula(Hu and Sugiyama, 1996):

$$z_* = 1048 \left[1 + 0.00124(\Omega_b h^2)^{-0.738}\right] \left[1 + g_1(\Omega_m h^2)^{g_2}\right], \tag{B.2}$$

where

$$g_1 = \frac{0.0783\,(\Omega_b h^2)^{-0.238}}{1 + 39.5\,(\Omega_b h^2)^{0.763}} \tag{B.3}$$

$$g_2 = \frac{0.560}{1 + 21.1\,(\Omega_b h^2)^{1.81}} \tag{B.4}$$

The comoving sound horizon at redshift z is given by

$$
\begin{aligned}
r_s(z) &= \int_0^t \frac{c_s\,dt'}{a} = cH_0^{-1} \int_z^\infty dz'\, \frac{c_s}{E(z')}, \\
&= cH_0^{-1} \int_0^a \frac{da'}{\sqrt{3(1 + \overline{R_b}\,a')\,a'^4 E^2(z')}},
\end{aligned}
\tag{B.5}
$$

where a is the cosmic scale factor, $a = 1/(1 + z)$, and $a^4 E^2(z) = \Omega_m(a + a_{\text{eq}}) + \Omega_k a^2 + \Omega_X X(z)a^4$, with $a_{\text{eq}} = \Omega_{\text{rad}}/\Omega_m = 1/(1+z_{\text{eq}})$, and $z_{\text{eq}} = 2.5 \times 10^4 \Omega_m h^2 (T_{CMB}/2.7\,\text{K})^{-4}$. The sound speed is $c_s = 1/\sqrt{3(1 + \overline{R_b}\,a)}$, with $\overline{R_b}\,a = 3\rho_b/(4\rho_\gamma)$, $\overline{R_b} = 31500\,\Omega_b h^2$ $(T_{CMB}/2.7\,\text{K})^{-4}$. We take $T_{CMB} = 2.725$.

The redshift of the drag epoch z_d is well approximated by Eisenstein & Hu (1998)

$$z_d = \frac{1291(\Omega_m h^2)^{0.251}}{1 + 0.659(\Omega_m h^2)^{0.828}} \left[1 + b_1(\Omega_b h^2)^{b2}\right], \tag{B.6}$$

where

$$b_1 = 0.313(\Omega_m h^2)^{-0.419} \left[1 + 0.607(\Omega_m h^2)^{0.674}\right], \tag{B.7}$$

$$b_2 = 0.238(\Omega_m h^2)^{0.223}. \tag{B.8}$$

There are only four independent parameters among these five and n_s is marginalized over in this study. Therefore, there are only three parameters left, $\{l_a, R, z_*\}$. CMB data

are included in our analysis by adding the following term to the χ^2 of a given model with $\Delta p_1 = l_a(z_*) - 302.35$, $\Delta p_2 = R(z_*) - 1.728$, and $\Delta p_3 = z_* - 1091.32$:

$$\chi^2_{CMB} = \Delta p_i \left[\text{Cov}^{-1}_{CMB}(p_i, p_j) \right] \Delta p_j, \tag{B.9}$$

where the inverse covariance matrix of (l_a, R, z_*) from WMAP7 (Komatsu et al., 2010) is given by (Wang, Chuang, & Mukherjee, 2011):

$$\text{Cov}^{-1}_{CMB} = \begin{pmatrix} 1.85710 & 25.9289 & -1.14325 \\ 25.9289 & 5963.26 & -99.3185 \\ -1.14325 & -99.3185 & 2.94429 \end{pmatrix} \tag{B.10}$$